Carbon materials for water desalination by capacitive deionization

Michio Inagaki[1,*], HUANG Zheng-hong[2,*]

（1. *Hokkaido University*, 228-7399 *Nakagawa*, *Hosoe-cho*, *Kita-ku*, *Hamamatsu* 431-1304, *Japan*;
2. *Key Laboratory of Advanced Materials (MOE)*, *School of Materials Science and Engineering*, *Tsinghua University*, *Beijing* 100084, *China)*）

Abstract: Recent developments on the capacitive deionization (CDI) technique for water desalination are reviewed with a focus on carbon as the electrode material. The capacity and rate of salt adsorption and charge efficiency of various types of CDI cells, i.e. flow-by, membrane, flow-through-electrode, and flowing electrode cells are compared. Various carbon electrode materials for capacitor-type and battery-type cells are discussed. The flowing electrode cell with the short-circuit operation mode seems to be the most promising one for practical applications.

Key words: Carbon materials; Capacitive deionization; Water desalination; Capacitor-type; Battery-type

1 Introduction

Water pollution and freshwater supply are two of the most serious environmental problems faced by human around the globe in the 21st century. Here, water desalination was reviewed and discussed by focusing on the carbon materials for capacitive deionization (CDI). The water desalination by this CDI process as well as solar steam-generation[1] are considered to be the most important technologies to address the increasingly necessity for global water scarcity.

CDI has attracted much attention over the past decade for the facile removal of ions from water as a method for removing dissolved salts from brackish water by their adsorption onto electrode surfaces mainly to form electric double-layers (EDLs), and now is one of the potential methods for desalination of drinking water. Basic concept of CDI is electrochemical adsorption of ions in water, the same as supercapacitors with aqueous electrolytes[2]; the cations of a salt, such as Na^+, are adsorbed onto the surface of the negative electrode and the anions, such as Cl^-, onto the positive electrode principally by forming EDLs. Therefore, porous carbons have been actively studied as the electrode materials and reviewed[2–9], due to the advantage such as the environmental friendliness, cost effectiveness, low energy consumption and convenient electrode regeneration. Its advantages in comparison with other desalination techniques, such as distillation, are followings: (1) CDI cells can be assembled in multiple pairs to construct a stack, which can be connected in parallel or in series to enhance the ion removal performances for practical applications. (2) Water desalination can perform quickly and the carbon electrodes can be regenerated easily by inversing the applied voltage. (3) The energy used for desalination can be partially recovered and utilized to charge another cell for desalination or storage medium such as supercapacitors for later use. Enormous progress has been made in the CDI research field and now it encompasses various cell architectures assembled with either capacitive electrodes or battery electrodes.

In this review, the electrochemical cells for water desalination are divided into 2 groups, either based on principally EDL formation on the surface of carbon electrodes (*i.e.*, capacitor-type cells) or principally Faradaic reaction with the carbon electrode (*i.e.,* battery-type cells), although a partial contribution of Faradaic reaction in the former cells and that of EDL formation in the latter cells are observed in many cases. The water desalination performances of these cells are compared and discussed on the bases on salt adsorption capacity and rate and charge efficiency.

Various CDI cells have been proposed, such as

Received date: 2023-01-27; **Revised date:** 2023-04-04

Corresponding author: Michio Inagaki, Professor. E-mail: im-ii@ace.ocn.ne.jp;
HUANG Zheng-hong, Professor. E-mail: zhhuang@mail.tsinghua.edu.cn

simple flow-by (FB) cell, flow-through-electrode (FTE) cell, membrane (M) cell and flowing-electrode (FE) cell, with some modifications, such as, cell using different carbon materials at the electrodes (asymmetric cell), chemical modification of the surfaces of the carbon electrodes (inverted cell), etc. In Fig. 1, 4 representative cell constructions, *i.e.*, simple FB-, M-(selecting cation-exchange membrane), FTE- and FE-CDI cells are schematically shown.

Fig. 1a shows a simple cell (FB-cell), which has been most frequently employed for the studies on CDI processes. A brackish water is forced to flow through the gap between 2 electrodes, where cations are electrochemically adsorbed onto the negative electrode and anions onto the positive electrode. The desalinated water is obtained at the outlet of the cell as an effluent. The capacity calculated from the change in the salt concentration of the effluent is a sum of 3 deionization mechanisms: (1) the adsorption due to the formation of EDLs on the surfaces of the carbon electrodes under electric field, (2) capturing of salt ions due to reversible Faradaic reaction with the surface functional groups of the carbon electrodes, (3) physical adsorption of salt ions onto the carbon surface without electric field. The first two occur under electric field, often being measured as a sum and so called electrosorption, which depend strongly on the applied voltage. The third, however, occurs without electric field and is mainly governed by the salt ions and the pore structure of carbon electrodes.

By inserting a cation-exchange membrane (CEM) in front of the negative electrode, as illustrated in Fig. 1b, salt removal efficiency is markedly improved (membrane CDI, M-CDI cell), because the cations can be selectively passed through the membrane and are subsequently adsorbed by the negative electrode without any interference of anions. Anion-exchange membrane (AEM) in the front of the positive electrode can also improve the electrosorption of anions. Using porous carbon electrodes, the brackish water was desalinated by passing through a pair of electrodes (flow-through-electrodes CDI, FTE-CDI cell, Fig. 1c), even a stack of electrode pairs, to obtain high efficiency of desalination because of a high opportunity of the contact between salt ions and electrode carbon surfaces. Flowing-electrode CDI cell (FE-CDI) is developed (Fig. 1d), where the fixed carbon electrodes is replaced by the flowing carbon particles by suspending the carbon particles in an aqueous solution, which flows through the channels carved on the current collectors. This system has some advantages, a continuous desalination process by coupling with the same cell for the desorption of adsorbates in the electrode carbon particles and a high removal efficiency from salted water with high concentration, because the flow-electrode can have infinite ion adsorption capacity.

In this review, the basic cell configurations of deionization devices are explained in the Section 1. In the Section 2, various carbon materials are introduced

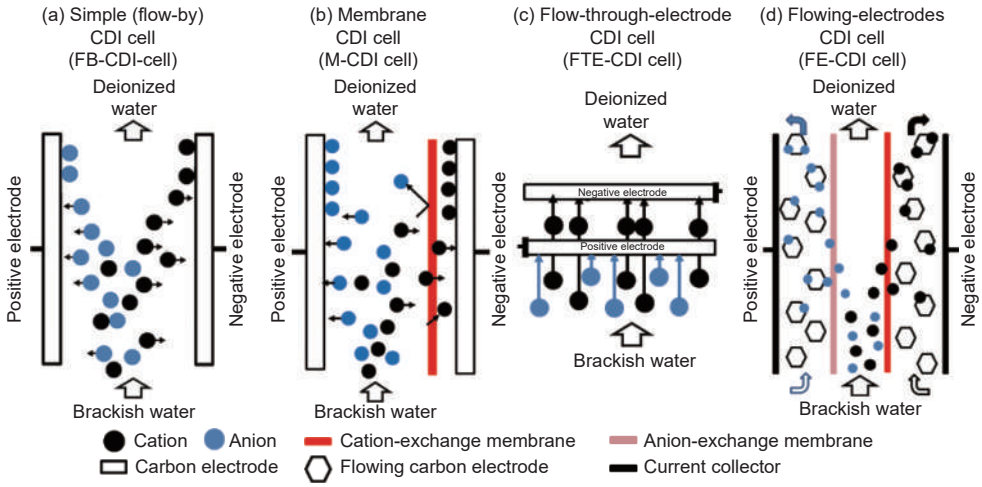

Fig. 1 Schematic illustrations of four representative CDI cells

by using NaCl as an applicable salt because most of investigations are using it and by focusing on capacitive contribution for the desalination, followed by the explanation on the application results on other cations and then discussed on the contribution of Faradaic reaction for salt ions adsorption, suggesting 2 adsorption mechanisms for salt ions for CDI process, the contributions of capacitive and of Faradaic adsorptions. Subsequently a comparison between different CDI cells is presented by discussing on the bases of ion-adsorption mechanisms with particular emphasis on the contribution of Faradaic reaction, and then introduced some modification of CDI cells, particularly on M-CDI cell and on operation modes of FE-CDI cell. In addition, a brief introduction of new proposals on CDI cells, although carbon materials for electrode of the cells have not been investigated in detail. In the Section 3, the battery-type CDI cells are shortly explained, because not many carbon materials had been applied. In the Section 4, co-generation of electric power in CDI process was shortly explained although only limited number of the papers have been published.

For the evaluation of performances of deionization, salt adsorption capacity (SAC), salt adsorption rate (SAR) and charge efficiency (CE) are mainly used in this review, even though there have been used many other parameters, such as energy consumption, removal efficiency, etc.

2　Carbon materials for capacitor-type cells

2.1　Performance for NaCl

Commercial granular activated carbons (AC) was applied as electrode material for a symmetric FB-CDI cell[10]. When granular AC was packed into a CDI cell as the electrodes without pressure, ion removal was very small because of high electric resistance of the AC electrodes. By compression of the AC onto the current collectors of a cylindrical cell, the amount of ion removal was significantly improved due to a drastic decrease in the electrical resistance. The SAC increased from 0.2 to 5.2 mg/g by compressing to 677 kPa at the applied voltage of 1.2 V, the AC thickness of 10 mm and the initial NaCl concentration of 10 mmol/L. During adsorption and desorption cycles (desalination and regeneration cycles) under pressure, the SAC was found to be stable between 9.6 and 10.3 mg/g.

N-doped hierarchically porous carbons were prepared from the powder mixture of potassium citrate (P) of 3 g, urea (U) of 3 g and ammonium citrate (A) of 0.6 g by grinding and following carbonization at 800 °C for 1 h in N_2 (coded as PC_{PUA})[11]. For comparison, the carbons were prepared from P without mixing U and A, followed by KOH activation with mass ratio of 5∶1 (coded as PC_P), and that from P mixed with U by KOH-activation with mass ratio of 1∶1 (PC_{PU}). The pore structure parameters of the resultant carbons are summarized in Table 1, and their SEM images in Fig. 2. These SEM images and pore structure parameters demonstrate that the resultant carbons are highly hierarchical. The precursors U and A were supposed to work as activation agents, being assisted by the formation of decomposition gases. CDI performances of these hierarchically porous carbons were investigated using a symmetric FB CDI-cell with NaCl solution. In Fig. 3a-c, the changes in SAC were shown as the functions of charging time, applied voltage and initial NaCl concentration for the resultant four carbons. The carbon PC_{PUA} delivered the

Table 1　Pore structure parameters of the porous carbons prepared from the mixtures of potassium citrate (P), urea (U) and ammonium citrate (A). Reprinted with permission from Ref. [11]. Copyright (2023) by Elsevier

Code	Precursors	S_{BET}/(m^2/g)	V_{total}/(cm^3/g)	V_{micro}/(cm^3/g)	V_{meso}/(cm^3/g)	V_{micro}/ V_{total} (%)	V_{meso}/ V_{total} (%)
PC_P	P	1159	0.66	0.48	0.18	73	27
PC_{PA}	P+A (5/1)	1668	0.90	0.52	0.38	58	42
PC_{PU}	P+U (1/1)	2785	1.65	0.81	0.84	49	51
PC_{PUA}	P+U+A (5/5/1)	3200	2.49	1.05	1.44	42	58

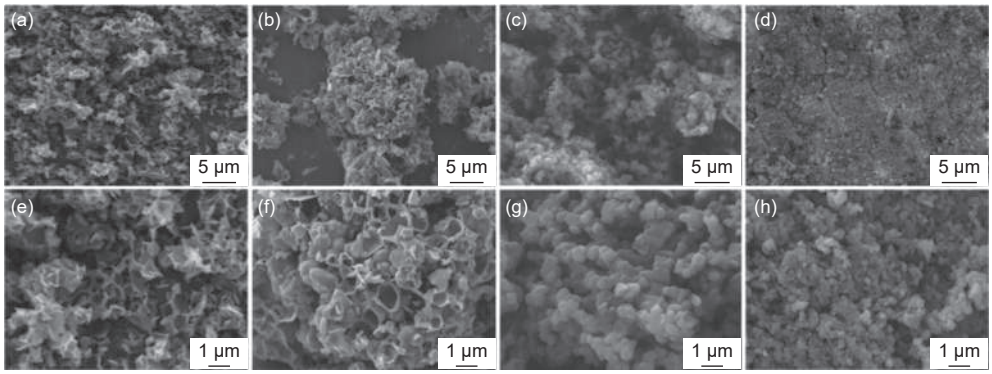

Fig. 2 SEM images of the carbons prepared from the powder mixture of potassium citrate (P), urea (U) and ammonium citrate (A) by carbonization at 800 °C. (a, e) PC_P, (b, f) PC_{PA}, (c, g) PC_{PU}, and (d, h) PC_{PUA}. Reprinted with permission from Ref.[11]. Copyright (2023) by Elsevier

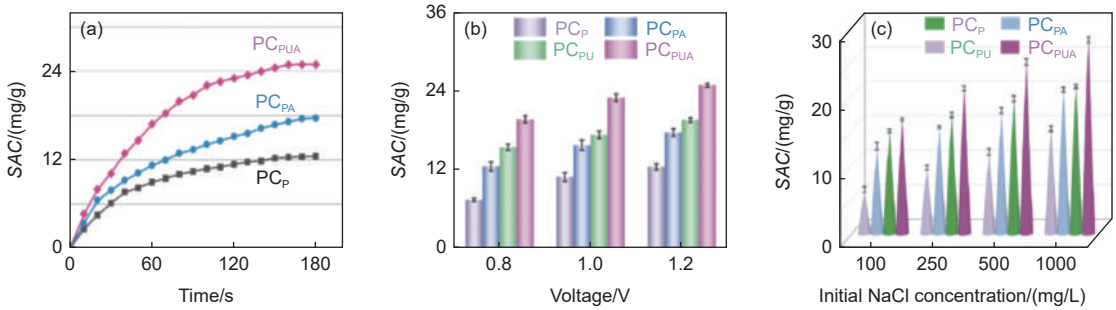

Fig. 3 CDI performance of the hierarchically porous carbons prepared from potassium citrate, urea and ammonium citrate by carbonization at 800 °C: the changes of SAC with (a) time, (b) applied voltage and (c) initial NaCl concentration. Reprinted with permission from Ref.[11]. Copyright (2023) by Elsevier

highest performances: SAC of 25 mg/g, SAR of 8.29 mg/g·min at 1.2 V and 500 mg/L NaCl concentration. It also exhibited a stable long-term cyclability with 88.7% SAC retention after 50 adsorption-desorption cycles.

Cubic pieces with a size of 50 m×50 m×5 m cut from a natural basswood block, which were carbonized at 1 000 °C for 6 h in Ar, followed by activation in CO_2 at 750 °C for 10 h[12]. Carbonized wood pieces with honeycomb-like texture were polished by sandpapers to obtain a thin sheet (membrane of 20 mm× 35 mm with a thickness of 1.2 mm. Sandwiching a spacer membrane between two wood-derived membranes, a symmetric FB-CDI cell with 1.0 mol/L NaCl solution was assembled. CDI performances measured on the electrode of carbonized wood-membrane were compared with those of a commercial AC. As shown in Fig. 4a, the membrane makes an effluent conductivity decrease rapidly down to 40 μS/cm from 200 μS/cm for the pristine solution, whereas the AC gives the effluent conductivity of 140 μS/cm, indicating a higher SAC of the carbonized membrane electrode. To decrease the conductivity down to 60 μS/cm, it needs only 32 min while the AC spends 180 min. For desorption (recovery of the conductivity up to 200 μS/cm), in addition, the membrane completes after 30 min, while the AC needs 68 min. The results demonstrate that the membrane electrode not only displays a high SAC but also a fast SAR together with a high desorption rate. The membrane exhibited a high areal SAC of 0.3 mg/cm^2 (a high volumetric SAC of 2.4 mg/cm^3, and a gravimetric SAC of 5.7 mg/g). Also, the good mechanical strength and water tolerance of the membrane electrodes improve the cycling stability, as shown the changes in conductivity and SAC in comparison with a commercial AC in Fig. 4b-c, respectively.

Cocoon wastewater (CW) obtained from a silk reeling factory, which contains silkworm cocoon waste (protein-content of 45 000-47 000 mg/L), was removed the suspended solid impurities by filtration, mixed with $ZnCl_2$ in its concentration of 0.5, 1.0, 1.5 and 2.0 mol/L, and then heated at 300 °C for 2 h to remove the moisture and tar, and finally heated at

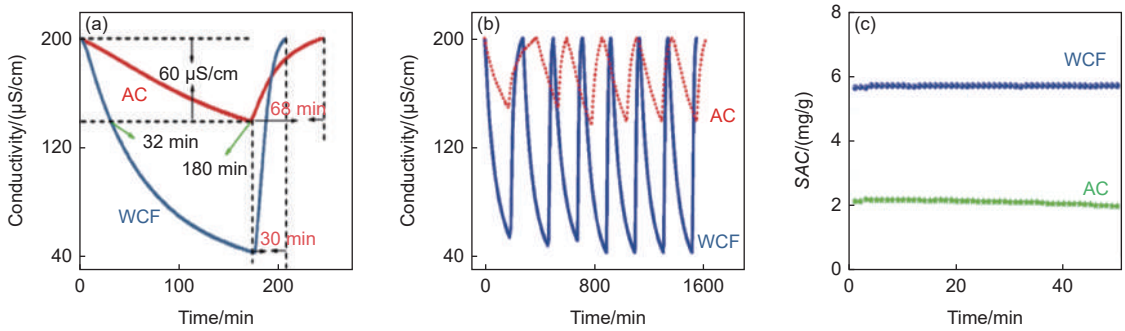

Fig. 4　CDI performance of the basswood-derived carbon thin section in comparison with an AC: (a) conductivity change during the first desalination/regeneration cycle, (b) conductivity and (c) SAC change with cycle. Reprinted with permission from Ref. [12]. Copyright (2018) by American Chemical Society

900 °C for 1 h in N_2 to obtain a black solid (coded as CWC-0.5-2.0)[13]. The resultant black solid was ground into powder, which was subsequently immersed into a 0.5 mol/L HCl solution to remove the zinc species. For comparison, pure cocoon waste (not wastewater) was also converted to carbon with the same condition (CWC-0.0). The final products were hierarchically porous, as shown pore structure parameters in Table 2. The CDI performances of these carbons were studied using a symmetric FB CDI cell with NaCl solution. The performances are shown in Fig. 5a-c. The carbon CWC-1.5 exhibits the highest SAC of 30.3 mg/g at the initial NaCl concentration of 500 mg/L and 1.2 V, whereas it does not have the highest S_{BET} (Table 2), which may attribute to the highest mesopore-content, V_{meso}/V_{total} (more than 70%). It exhibited high reusability and stability as only 3% reduction in SAC even after the 50th cycle.

A hierarchically porouls carbon foam consisting of entangled hollow filaments were prepared from cultivated mushroom mycelium (MDC)[14]. Mycelium was washed with de-ionized water and dried at 60 °C overnight and then carbonized at 500 °C for 2 h, followed by mixing with KOH in carbonized mycelia/KOH mass ratio of 1∶2 and carbonized and activated at 800 °C for 3 h. For comparison, sporophores was also carbonized and KOH-activated (SDC). In Fig. 6a, SEM images of the pristine mycelium is

Table 2　Pore structure parameters of the carbons derived from cocoon wastewater. Reprinted with permission from Ref. [13]. Copyright (2023) by Elsevier

Code	$ZnCl_2$ concentration/(mol/L)	S_{BET}/(m^2/g)	V_{total}/(cm^3/g)	V_{micro}/V_{total}(%)	V_{meso}/V_{total} (%)	V_{macro}/V_{total}(%)
CWC-0.5	0.5	1295	0.69	73.1	26.7	0.2
CWC-1.0	1.0	1311	0.74	69.5	30.3	0.2
CWC-1.5	1.5	1 282	1.11	23.1	75.5	1.4
CWC-2.0	2.0	911	1.21	16.1	69.1	14.8
CWC-0.0	0.0	1409	1.14	31.0	62.7	6.3

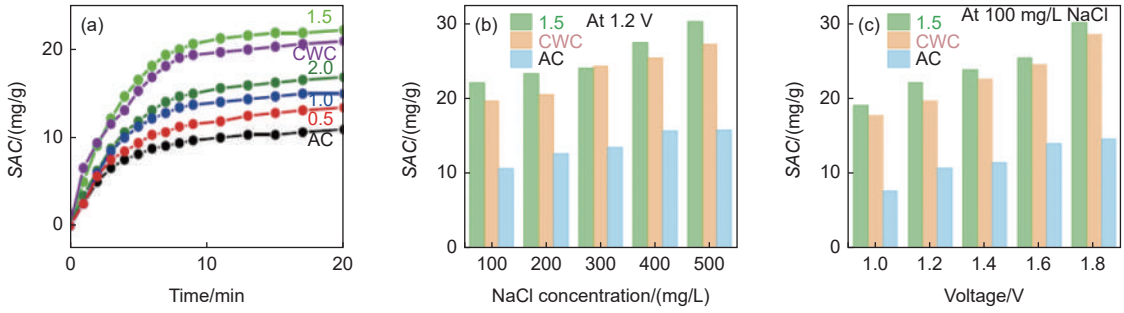

Fig. 5　CDI performance of the carbons derived from cocoon wastewater (CW) using different $ZnCl_2$ concentrations (0.0-2.0 mol/L) in CW aqueous solutions in comparison with a commercial activated carbon (AC): (a) SAC changes with time for the carbons prepared by using different $ZnCl_2$ concentrations in comparison with AC, (b) effects of the NaCl initial concentration and (c) applied voltage on SAC for the carbons CWC-1.5 and CWC-0.0. Reprinted with permission from Ref. [13]. Copyright (2023) by Elsevier

shown with the illustration of mycelium and sporophores of mushroom. In Fig. 6b, SEM image of carbonized mycelium is shown, revealing entangled texture of hollow filaments. N_2 adsorption-desorption isotherms are shown for the carbons MDC and SDC in Fig. 6c, with pore-size distribution (inset), revealing that the mycelium results in the carbon with more developed hierarchical pore structure. The CDI performances of these carbons (MDC and SDC) are shown in Fig. 7a and b, as the time changes of SAC and the plots of SAR against SAC (CDI Ragone plots), respectively.

The biochar obtained mainly from Douglas-fir wood chips at 900-1 000 °C, which was activated with KOH at 900 °C for 2 h in Ar (activated biochar AcB), functionalized by stirring AcB with sodium nitrite and *p*-phenylene diamine in water (amine group functionalization, AmB). A mixture of AcB and AmB was coated with Nafion at biochar/Nafion mass ratio of 9∶1 (NfB)[15]. By coupling these three kinds of carbons for electrode materials, symmetric and asymmetric FB-CDI cells were assembled and their desalination performances were compared. SAC and CE are listed in Table 3. The asymmetric cell of NfB at the

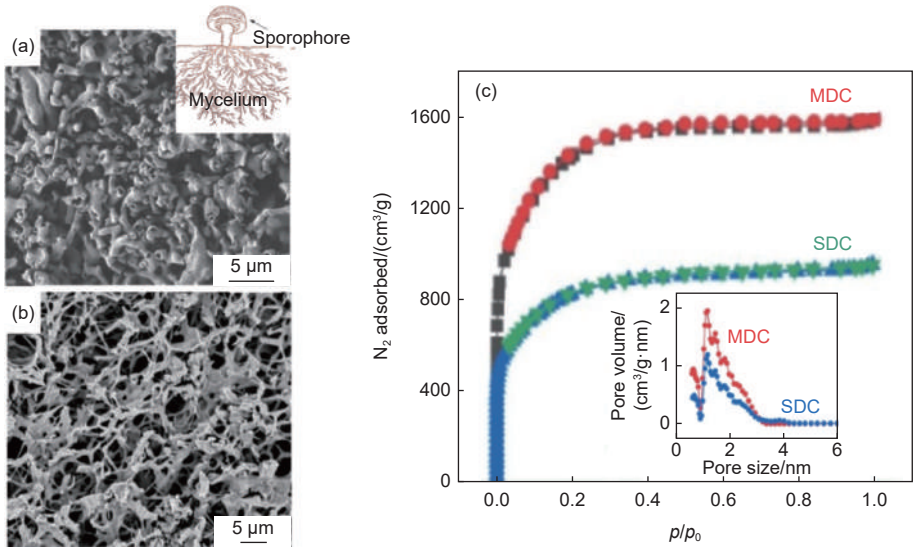

Fig. 6 Carbon derived from mushroom mycelium using $ZnCl_2$ template carbonization/KOH-activation at 800 °C (MDC): (a) SEM image of the pristine mycelium with illustration, (b) that of the carbon after activation, and (c) N_2 adsorption-desorption isotherms at 77 K with the pore-size distribution for MDC and SDC (inset). Reprinted with permission from Ref. [14]. Copyright (2022) by Elsevier

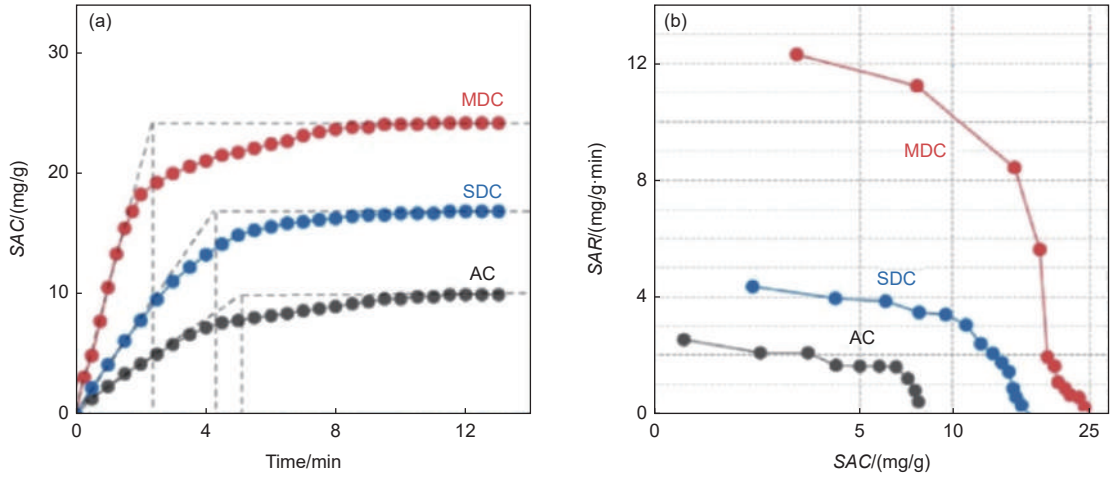

Fig. 7 CDI performances of the carbons derived from mushroom mycelium (MDC) and sporophores (SDC) in a symmetric FB CDI cell in comparison with a commercial activated carbon (AC): (a) changes in SAC with time at the applied voltage of 1.4 V and the initial NaCl concentration of 500 mg/L, and (b) CDI Ragone plots. Reprinted with permission from Ref. [14]. Copyright (2022) by Elsevier

positive electrode and AmB at the negative electrode (AmB//NfB cell) delivers the largest SAC and CE, much larger than the symmetric cell AcB//AcB, revealing that the surface modification by amination of the negative electrode and Nafion coating of the positive electrode are effective for the improvement of desalination performances.

A three-dimensionally ordered honeycomb-like N-doped porous carbon (3D-PC) using ZIF-8 was synthesized using polystyrene microspheres as a sacrificial template at 800 °C for 3 h[16]. ZIF-8 was uniformly anchored on both sides of graphite oxide (GtO) nanosheets to produce 2D ZIF-8/GtO nanoarchitectures, which could be converted by high temperature treatment to the composite of N-doped ZIF-8-derived carbon with rGtO flake (N-doped carbon/rGtO composite), followed by P-doping with phytic acid of N-doped carbon to obtain N/P-co-doped carbon/rGtO composite (NPC/rGtO composite)[17]. The composite NPC/rGtO delivered a high SAC of 39.34 mg/g in 1 000 mg/L NaCl solution at 1.2 V. In 250 mg/L solution at 1.2 V, the SAC of NPC/rGtO reached 27.36 mg/g, much higher than 20.53 mg/g for NC/rGtO and 15.93 mg/g for N-doped carbon (ZIF-8-derived carbon without GO). MnV_2O_6-loaded rGtO (MVO/rGO) was synthesized by hydrothermal treatment of the mixture of $Mn(CH_3COO)_2$, NH_4VO_3 and GO with sodium dodecyl sulfate (surfactant) at 180 °C for 18 h and used for the construction of a symmetric FB-CDI cell[18]. It delivered the SAC of 49.3 mg/g at the applied voltage of 1.4 V in the 1 000 mg/L NaCl solution and excellent long-term cycle stability up to 50 cycles. N-doped porous carbon with bowl-like particle morphology was prepared from ZIF-8 using carboxylate-terminated polystyrene microspheres as template by carbonization at 850 °C for 3 h in N_2[19]. The resultant carbon consisted of the bowls having the size of 150-250 nm with the wall thickness of 20-45 nm. The carbon delivered the SAC of 28.06 mg/g and SAR of 1.56 mg/g·min at 1.2 V in 0.5 g/L NaCl solution with about 90% SAC retention after 20 desalination/regeneration cycles.

Grafting SiO_2 nanoparticles on activated carbon cloth (ACC) surface was effective to enhance CDI performances[20]. A commercial ACC was immersed in a mixture of tetraethyl orthosilicate (TEOS) and ammonia in equal volume ratio for 2 h, using different concentrations of TEOS solutions, 0-90 mmol/L, followed by washing with ethanol and drying in a desiccator to obtain SiO_2-nanoparticle-grafted ACCs. CDI performances were determined using a symmetric FB-CDI cell with NaCl solutions of different concentrations. In Fig. 8a-c, an effect of the concentration of the TEOS solution on capacitance measured in a three-electrode cell with 0.5 mol/L NaCl aqueous electrolyte, and desalination efficiency and SAR measured in a symmetric FB-cell with 2×10^{-4} NaCl solution, respectively. The SiO_2-nanoparticle-grafted ACC obtained using 45 mmol/L TEOS solution exhibited the highest CDI performances with desalination efficiency of 70% and SAR of 0.075 mg/cm^2 min. The pristine ACC had S_{BET} of 1 043 m^2/g including S_{micro} of 742 m^2/g, while even after SiO_2-grafting S_{BET} kept a value of 1 040 m^2/g, including S_{micro} of 742 m^2/g. The enhancement in desalination performances of the ACC was suggested to prevent the substantial oxidation of the electrode carbon surfaces.

N-doped porous carbons with hydrangea-like particles were prepared from NH_2-MIL-53(Al), (*i.e.*, $AlO_4(OH)_2$ as clusters with 2-aminoterephthalic acid

Table 3　SAC and CE of the FB-CDI cells using the carbons derived from the biochar, AcB, AmB, NfB as the electrode materials. Reprinted with permission from Ref. [15]. Copyright (2021) by Elsevier

Cell configuration			*SAC*/(mg/g)	*SAC*/(mmol/g)	*CE*/%
	Positive	Negative			
Symmetric	AcB	AcB	6.01	0.103	21.42
	NfB	AcB	7.33	0.125	22.59
Asymmetric	AcB	AmB	5.31	0.090	17.01
	NfB	AmB	9.25	0.156	27.81

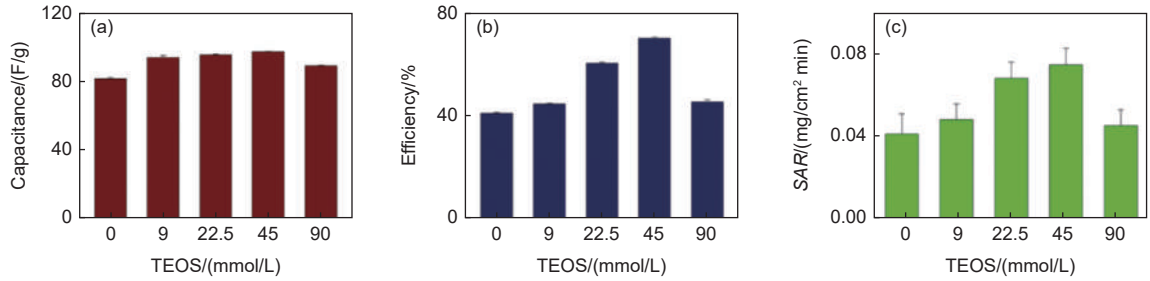

Fig. 8 SiO_2-nanoparticle-grafted ACCs: TEOS-concentration dependence of (a) capacitance of a three-electrode cell with 0.5 mol/L NaCl aqueous electrolyte, (b) desalination efficiency and (c) *SAR* measured in a symmetric FB-cell with 2.0×10^{-4} NaCl solution. Reprinted with permission from Ref. [20]. Copyright (2022) by Elsevier

as organic ligands) by carbonization at 800, 900 and 1 000 °C for 5 h in N_2, followed by washing with HF and distilled water[21]. The carbon obtained at 900 °C delivered the highest pore structure parameters (S_{BET} of 1 369 m^2/g with V_{total} of 0.86 cm^3/g including V_{micro} and V_{meso} of 0.22 and 0.39 cm^3/g, respectively) and with N-content of 0.56 at% mostly at pyrrolic configuration. It also delivered the highest CDI performances: SAC of 21.17 mg/g, CE of 0.83% in 500 mg/L NaCl solution at an applied voltage of 1.2 V with SAC retention of 86% after 15 desalination/regeneration cycles. Co/N-co-doped porous carbons were prepared from a mixture of *D*-glucose with $Co(NO_3)_2$ in $Co(NO_3)_2$/glucose mass ratio of 20, 30 and 50 by carbonization at 600 °C for 2 h in N_2 using a molten salt LiCl/KCl (45/55 by weight) as a template[22]. The carbon obtained using the mass ratio $Co(NO_3)_2$/glucose of 20 delivered a high SAC of 58.82 mg/g at 1.4 V in a NaCl solution with 824 mg/L concentration and a high cycling stability with no obvious decrease in SAC during 100 desalination/regeneration cycles.

Inclusion of rGtO nanoflakes into the matrix of carbon nanofibers was experimentally demonstrated to be effective for an improvement of CDI performances[23–24]. Carbon nanofiber (CNF) webs prepared from a DMF solution of PAN with GtO nanoflakes by electrospinning, followed by stabilization at 280 °C for 2 h in air and then carbonization/activation at 800 °C for 0.5 h in a 30% (volume) steam flow. The resultant rGtO-containing CNF web delivered SAC of 13.2 mg/g for 450 mg/L NaCl solutions, much improved from 9.4 mg/g for CNF web without rGtO[23]. Composite of rGtO with N-doped soybean-derived carbons prepared from a soy milk of 100 mL mixed with 200 mg GtO flakes and 0.3 g lactose by pre-carbonization at 250 °C in air and then carbonization/activation at 850 °C for 2 h after mixing KOH[25]. The resultant composite delivered the SAC of 38.4 mg/g with 1 000 mg/L NaCl solution, larger than N-doped soybean-derived carbon without rGtO (28.6 mg/g) in a symmetric FB-cell, whereas the latter had larger S_{BET} of 2 994 m^2/g than the former (1 286 m^2/g).

Covering of ACF by single-layered GnO nanoflakes with N-doped porous carbon was very effective to enhance the CDI performances[26]. The commercial ACF and single-layered GnO were selected, and N-doped porous carbon was prepared from the mixture of sucrose, melamine and $CaCO_3$ (template) in 2∶2∶1 ratio by carbonization at 800 °C for 2 h in N_2. The composites of ACF with single-layered GnO and N-doped porous carbon were prepared by coating *via* NMF solution dispersing single-layered GnO, porous carbon, acetylene black and PVDF in the ratio of 16∶8∶1∶1 followed by drying at 80 °C. The composites of N-doped carbon/ACF and single-layered GnO/N-doped carbon/ACF are shown by SEM images with the pristine ACF in Fig. 9, revealing that N-doped porous carbon and single-layered GnO are covering the surfaces of individual carbon fibers. SAC measured using a symmetric FB CDI cell are shown in Fig. 10a by comparing among the resultant composites, *i.e.*, N-doped porous carbon/ACF, single-layered GnO/ACF and single-layered GnO/N-doped carbon/ACF and the pristine ACF. The composite single-layered GnO/N-doped carbon/ACF delivers the highest SAC (19.7 mg/g), revealing that simultaneous

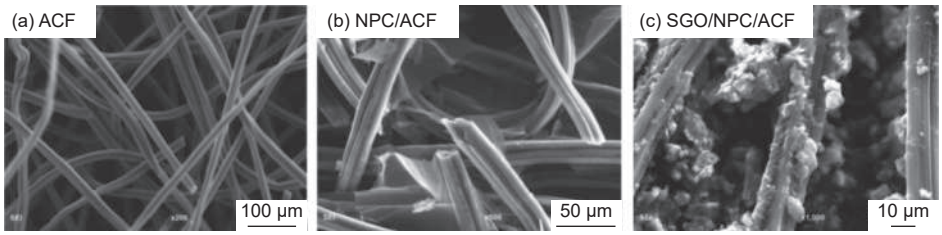

Fig. 9　SEM images of the composites of the ACF with N-doped porous carbon (NPC) and single-layered GnO nanoflakes: (a) the pristine ACF, (b) the composite NPC/ACF and (c) single-layered-GnO/NPC/ACF composites. Reprinted with permission from Ref.[26]. Copyright (2022) by Elsevier

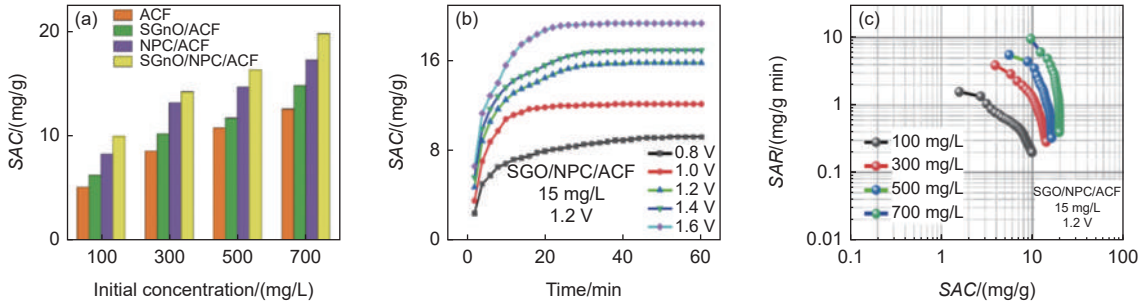

Fig. 10　CDI performance of the composites of the activated carbon fibers (ACF) with N-doped porous carbon (NPC) and single-layered GnO nanoflakes: (a) SAC as a function of initial NaCl concentration on 4 composites, (b) change of SAC with time and (c) CDI Ragone plot for the composite single-layered-GnO/NPC/ACF. Reprinted with permission from Ref.[26]. Copyright (2022) by Elsevier

coating of single-layered GnO and N-doped porous carbon results in the significant enhancement of SAC, whereas its S_{BET} became much smaller (1 155 m^2/g) than the pristine ACF (2 079 m^2/g). On the composite single-layered GnO/N-doped carbon/ACF, the effect of applied voltage during CDI process is shown in Fig. 10b and CDI Ragone plot in Fig. 10c.

The negatively charged carbon nanofibers (negative-CNFs) were prepared by electrospinning of a mixture of polyacrylonitrile (PAN) with poly-methylmethacrylate (PMMA) in 4 by mass ratio and the positively charged nanofibers (positive-CNFs) were prepared by heat-treatment at 800 °C for 1 h after impregnating the negative-CNFs into 2 mol/L $ZnCl_2$ solution, followed by washing with 0.5 mol/L HCl and water[27]. The potential of zero charge (E_{PZC}) was determined to be 0.32 and −0.68 V for the N-CNFs and P-CNFs, respectively, the CNFs obtained from PAN without PMMA (CNFs) exhibited E_{PZC} of 0.01 V (almost neutral). Asymmetric FB-CDI cells were assembled by using the P-CNF at the negative electrode and the N-CNF at the positive electrode (N-CNF//P-CNF cell), together with the reversed cell (P-CNF//N-CNF cell), and a symmetric FB-cell (N-CNF//N-CNF), of which the CDI performances were compared. As shown NaCl concentration kinetics in Fig. 11a, the asymmetric P-CNF//N-CNF cell exhibits an extremely faster and larger NaCl concentration changes, suggesting a high SAC and SAR. In Fig. 11b, SAC and CE are compared on 3 CDI cells, SAC and CE of the P-CNF//N-CNF cell reach 30.4 mg/g and 1.0 mg/g·min, respectively, much higher than other two cells using the same carbon electrodes.

Addition of cobalt and titanium carbides nanoparticles into the matrix of CNFs was shown to be effective to enhance the CDI performances[28]. The composite Co-TiC@CNF was synthesized by electrospinning of an acetic acid/ethanol (1/1) solution of PVP, titanium (IV) isopropoxide and cobalt acetate, following carbonization at 950 °C for 6 h in Ar flow. The resultant CNFs had smooth surface, containing both carbides as crystalline nanoparticles, of which weight percentages of C, Ti and Co were determined by EDX analyses to be 56.12%, 37.68% and 6.20%, respectively. The CDI performances of the composite (Co-TiC@CNF), the pristine CNFs and TiC were measured in a symmetric FB-cells with 50 mg/L NaCl solution at different potentials as 0.8, 1.0 and 1.2 V (Fig. 12). Rapid decrease in conductivity of the effluent by the composite in Fig. 12a suggests high SAC

and SAR of the composite than the pristine CNFs and TiC. SAC depends strongly on the potential applied, as shown in Fig. 12b, revealing that the composite gives the highest SAC at all potential ranges examined. The composite exhibits a stable desalination-regeneration cycles with rapid concentration changes (Fig. 12c). Coating of the layered double hydroxides (LDHs) of Ni and Mn on the surface of CNFs also showed an improvement in the CDI performances[25]. CNFs were prepared from PAN-based electrospun nanofibers by stabilization at 280 °C for 2 h, followed by carbonization at 800 °C for 2 h in N_2. CNFs were immersed into a mixed solution of $NiCl_2$ (4.5 mmol/L), $MnCl_2$ (1.5 mmol/L), and NH_4F (18 mmol/L) under stirring, followed by drop-wise addition of NaOH (12 mmol/L) and NaCl (0.5 mol/L) and aged at room temperature for 12 h with O_2 bubbling to obtain LDH-coated CNF composite. The composite delivered SAC of 72.04 mg/g and a high SAR of 0.5 mg/g·s with the SAC retention of about 90% after 35 desalination-regeneration cycles.

2.2 Performance for different salts

N-doped carbon microspheres with vertically aligned carbon nanosheets were prepared from polyimide (PMDA/EDA) by refluxing its precursors solution, followed by carbonization at 800 °C in N_2 and activation at 800 °C for 2 h using KOH/carbon mass ratio of 4[29] (Fig. 13a). CDI performances of the symmetric FB-cell with this carbon was studied in a flow of NaCl and LiCl solutions with 500 mg/L concentrations. As shown in Fig. 13b and c. SAC, CE and energy consumption of the carbon depended strongly on the potential applied: SAC of 14.46 mg/g and CE of 69% with the highest energy consumption of about 160 Wh/m^3 for NaCl, while much smaller SAC of 6.76 mg/g for LiCl. Cycling stability of the cell was

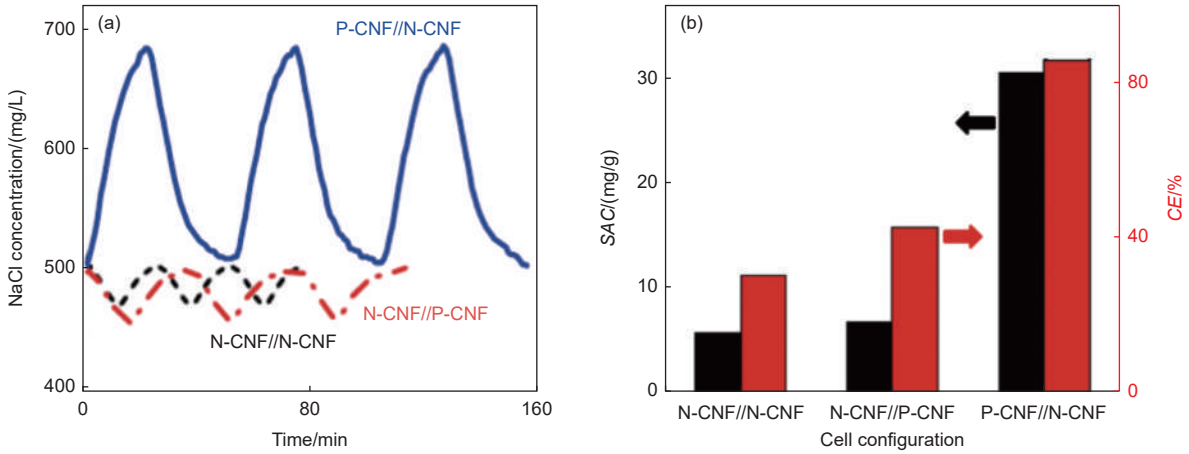

Fig. 11 Desalination performance of CDI cells using PAN-based carbon nanofibers (CNFs), symmetric FB-cell, N-CNF//P-CNF and asymmetric FB-cell, P-CNF//N-CNF as the electrode materials: (a) kinetics of NaCl concentration changes and (b) comparison of *SAC* and *CE* for three cells. Reprinted with permission from Ref.[27]. Copyright (2021) by Elsevier

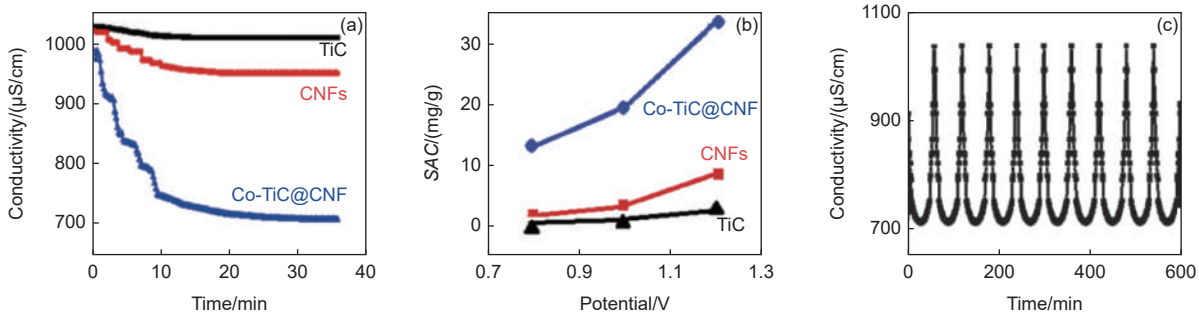

Fig. 12 CDI performance in a flow of NaCl solution with 15 mL/min rate for the composite Co-TiC@CNF, the pristine CNFs and TiC: (a) changes in conductivity of NaCl effluents, (b) dependences of SAC on the applied potential and (c) desalination-regeneration cycling of the composite at 1.2 V. Reprinted with permission from Ref.[28]. Copyright (2022) by Elsevier

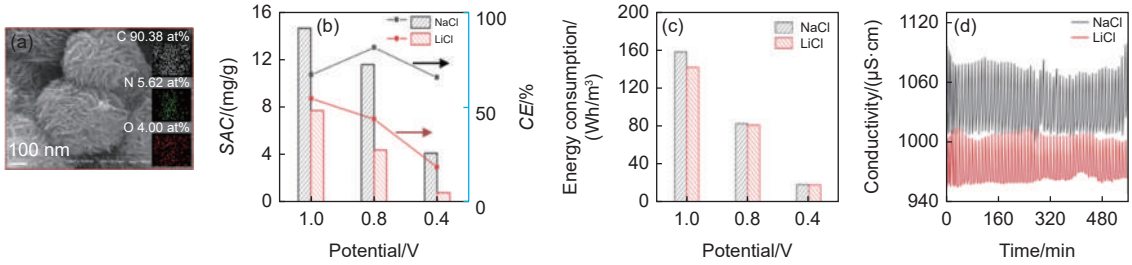

Fig. 13　CDI performance of N-doped carbon microspheres with vertically aligned carbon nanosheets prepared from a polyimide by carbonization at 800 °C and activated with KOH for NaCl and LiCl aqueous solutions: (a) SEM image, (b) changes in SAC and CE with potential applied, (c) changes in energy consumption with potential applied, and (d) conductivity change with cycling up to 56 cycles. Reprinted with permission from Ref.[29]. Copyright (2021) by Elsevier

confirmed up to 56 cycles (Fig. 13d).

A composite of PAN-based nanofibers electrospun from PAN containing graphene quantum dots (dots/PAN of 3/4 by weight) with ZIF-8 was synthesized by an *in-situ* growth method[30]. The composite was stabilized at 280 °C and carbonized at 800 °C for 2 h in Ar (CNF_{ZIF}), which had S_{BET} of 416 m^2/g with V_{total} of 0.215 cm^3/g including V_{micro} of 0.140 cm^3/g and total N-content of 13 at.% mainly in pyridinic and pyrrolic configurations. In Fig. 14a, the SAC of the composite for NaCl increases with increasing its initial concentration, from 8.59 mg/g for 100 mg/L to 19.69 mg/g for 800 mg/L. SAR also increased with increasing NaCl concentration. The composite has relatively high SACs, 27.19, 25.35 and 20.46 mg/g for other salts, $CaCl_2$, $MgCl_2$ and KCl, respectively (Fig. 14b). It also exhibited an excellent cyclability, a high retention of SAC as 97% after 30 desalination/regeneration cycles (Fig. 14c)

An electrode of reduced graphite oxide sheets on Ni foam (rGtO/Ni composite), which was a binder-free and self-standing, was tested as the electrodes of FB-CDI cell[31]. The composite was prepared by immersing a Ni foam into a GtO suspension synthesized by Hummers' method. To obtain the optimized loading of GtO flakes, the immersing process was repeated several times. The composite obtained was freeze-dried for 24 h and then heat-treated at 800 °C. The SAC of the composite obtained after two-times immersion was measured to be 22.3 mg/g in 5.0×10^{-4} NaCl solution at the applied voltage of 0.9 V with SAC retention of 65% after 200 consecutive cycles (9 days). A free-standing N-doped rGtO foam was prepared using polystyrene (PS) spheres (about 500 nm diameter) as template by electrostatic self-assembly of sequential coating of positively-charged GtO flakes and negatively-charged GtO onto negatively-charged PS surface[32] (Fig. 15a). The resultant GtO/PS composites contained about 8% (mass fraction) GtO and were compressed under about 1.0 MPa/cm^2 pressure to obtain membrane. It was annealed at 600 °C for 4 h in NH_3 and further annealed at 800 °C for 1 h to dope N. For comparison, free-standing rGtO foam without N-doping was prepared. The N-doped GtO foam delivered SAC of 21.8 mg/g at 1.8 V in 100 mg/L NaCl solution with the SAC retention of about 95% after 10

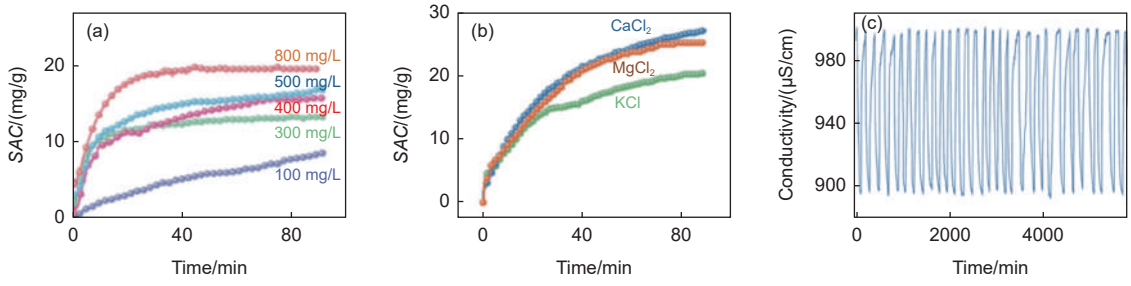

Fig. 14　CDI performance of the composite CNF_{ZIF}: (a) SAC for NaCl solutions with different concentrations (100-800 mg/L, (b) SACs for 5 mmol/L KCl, $CaCl_2$ and $MgCl_2$ solutions, and (c) cycle performance for 500 mg/L NaCl solution at 1.2 V[30]

desalination/regeneration cycles. It also has certain applicability towards other salts. At 1.2 V and 500 mg/L concentration of the salt solution, its SAC is about 15.2, 14.2, 13.1 and 12.5 mg/g for KCl, NaCl, $CaCl_2$ and $MgCl_2$, which is probably depending on the cation hydration radius (Fig. 15a). The Ragone plot (SAR *vs* SAC for carbon electrode) shown in Fig. 15b demonstrates that the SAC and SAR are the higher as the smaller the hydration radius of cation is.

Symmetric FB-CDI cells were constructed from the porous carbons derived from a metal-organic framework (MOF), ZIF-8, of which CDI performances were investigated in 250 mg/L saline solution under a flow rate of 25 mL/min at 1.2 V[33]. Nanoparticles composed of the core of ZIF-8 with *p*-aminophenol and formaldehyde (AF) shell (ZIF-8@AF nanocomposites) were prepared. ZIF-8@AF nanocomposite was carbonized at 900 °C for 3 h in N_2 to obtain N-doped eave-like porous carbon (coded by N-EPC) and then rinsed by 1 mol/L HCl, water and ethanol several times. N-EPC was mixed with phytic acid (inositol hexaphosphate, AP) in ethanol/H_2O mixed solution and then carbonized at 900 °C for 3 h in N_2 to get N/P-co-doped carbon (NP-EPC). In comparison, ZIF-8 was carbonized under the same conditions without adding AF (ZIF-8-C). Pore structure parameters and elemental compositions of the carbons derived from ZIF-8 are listed in Table 4. Three carbons possess almost the same S_{BET} of about 1 000 m^2/g, but V_{micro} decreases by carbonization of ZIF-8 with AF and (AF+AP) (in other words, by N-doping and N/P-co-doping, respectively), suggesting the increase in V_{meso}. The NP-EPC has S_{BET} of 1 166 m^2/g and is mesopore-rich, the percentage of mesopore being supposed to be about 82%. The carbonization of ZIF-8 with AF is supposed to be not effective for N-doping for the resultant carbon (Table 4). CDI performance is shown in Fig. 16a by plotting SAR against SAC for these carbons, in which NP-EPC delivers the highest SAC and fastest SAR, suggesting the highest CE. Specifically, it was determined as 50.7% for NP-EPC, 45.3% for N-EPC, and 37.7% for ZIF-8-C. The CDI performances of NP-EPC carbon electrode for other cations, K^+ and Ca^{2+}, are compared to those for NaCl in Fig. 16b. The SAC of NP-EPC for KCl is 22.24 mg/g (0.30

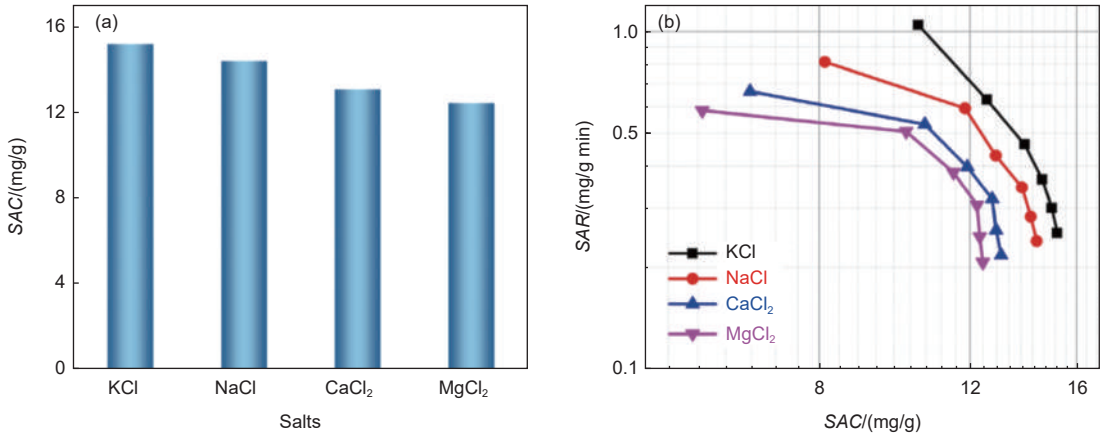

Fig. 15 CDI performances of the free-standing N-doped rGtO foam prepared using polystyrene spheres template for different salts: (a) *SAC* and (b) Ragone plot. Reprinted with permission from Ref.[32]. Copyright (2022) by Elsevier

Table 4 Pore structure parameters and elemental compositions of the carbons derived from ZIF-8 itself, and ZIF-8 with AF and (AF+AP) (N-EPC and NP-EPC)[33]

Carbon	Pore structure parameters				Elemental composition/at%				
	$S_{BET}/(m^2/g)$	$V_{total}/(cm^3/g)$	$V_{micro}/(cm^3/g)$	V_{micro}/V_{total}	C	O	N	P	N/P ratio
ZIF-8-C	1044	0.49	0.45	0.92	78.1	6.8	15.1		
N-EPC	1066	0.60	0.28	0.47	84.5	5.9	8.6		
NP-EPC	1166	0.72	0.13	0.18	78.6	16.8	2.9	1.7	1.71

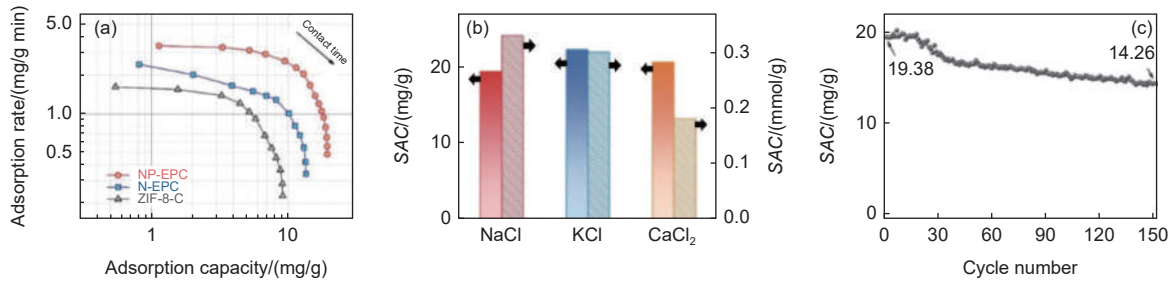

Fig. 16　Performances of symmetric FB-CDI cells using electrodes of the carbons derived from ZIF-8, ZIF-8-C, N-EPC and NP-EPC: (a) CDI Ragone plots in NaCl solution, (b) adsorption capacities and rates of NP-EPC for different salts, and (c) cycle performance of NP-EPC in 500 mg/L NaCl solution at 1.2 V[33]

mmol/g), larger than those of NaCl (19.38 mg/g, 0.33 mmol/g) and for $CaCl_2$ (20.59 mg/g, 0.18 mmol/g). The NP-EPC can accomplish the capacity retention of around 74% after 150 charging-discharging cycles (Fig. 16c).

Composites of rGtO flakes with λ-MnO_2 could adsorb Li^+ selectively by using it at the positive electrode and AC at the negative electrode of an asymmetric FB-CDI cell[22]. The composites were prepared by mixing rGtO (0.1, 0.2 or 0.5 g) with 1.732 g $Mn(NO_3)_2{\cdot}4H_2O$ in isopropanol and then adding 0.6 g Li_2O_2 under stirring for 12 h at room temperature to obtain λ-MnO_2/rGtO foams as the precipitates, which were washed, dried at 60 °C and then annealed at 200 °C in air for 3 h. The composite λ-MnO_2/rGtO prepared using 0.2 g rGtO showed the highest SAC for LiCl. The performances of this composite for different salts, LiCl, NaCl, KCl, $MgCl_2$ and $CaCl_2$ are shown in Fig. 17. SAR and SAC for LiCl are much higher than SACs for other salts, SAC in a single salt solution for Li^+ reaching 601 μmol/g, which is 3.2, 6.8, 5.3 and 3.7 times of SACs for Na^+, K^+, Mg^{2+} and Ca^{2+}, respectively (inset of Fig. 17a), revealing a high selectivity for Li^+ of the composite. In Fig. 17b, SAC for Li^+ (Li^+-SAC) and the ratio of adsorption efficiencies for Li^+ and Mg^{2+} (corresponding to separation factor) are shown as a function of the concentration ratio $C_{Mg^{2+}}/C_{Li^+}$ (Li^+ concentration is kept at 5 mmol/L). At the concentration ($C_{Mg^{2+}}/C_{Li^+}$ ratio of 1, the composite delivers a similar Li^+-SAC (411.7 μmol/g) to that of single-salt solution and the separation factor is near to 6.8. Even in the mixed solution with a concentration ratio as high as 30, the composite still keeps the Li^+-SAC of 215.5 μmol/g with the separation factor of 20.3. The advantage of this composite is also demonstrated by the results on SAC of the composite from a synthetic Salt Lake brine (23.48 mmol/L Li^+, 120.83 mmol/L Mg^{2+}, 256.4 mmol/L Na^+, 47.83 mmol/L K^+ and 0.57 mmol/L Ca^{2+}). In Fig. 17c, Li^+-SAC being kept at 206 μmol/g, much higher than that of Mg^{2+} (25 μmol/g). The composite exhibited a stable cyclability with SAC retention of about 75% after 30 cycles, much improved from 43% retention for λ-MnO_2 (without rGtO).

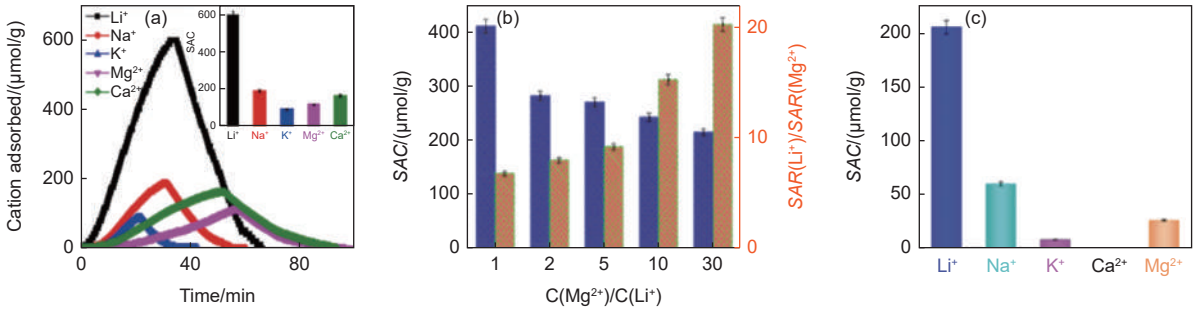

Fig. 17　CDI performances of λ-MnO_2/rGtO composite prepared using 0.2 g rGtO for different salts: (a) cations adsorbed with time from 10 mmol/L single-salt solutions with SAC for different cations (inset), and (b) dependences of SAC for Li^+ and of the ratio of adsorption ratio (adsorption efficiency) SAR for Li^+ to that for Mg^{2+} against concentration ratio of Mg^{2+} to Li^+ in a mixed solution and (c) SACs measured in a synthetic salt lake brine. Reprinted with permission from Ref. [22]. Copyright (2022) by Elsevier

2.3 Contributions of Faradaic reactions to cell performances

Capacitive storage of ions (non-Faradaic process) is the principal reaction in the different types of CDI cells, which are evaluated by measuring SAC and SAR of the ions in the brackish water. However, Faradaic reactions (*i.e.*, redox reactions on the surfaces of the carbon electrodes) were pointed out possibly to lead to the formation of chemical byproducts, such as H_2O_2, pH fluctuations of the produced deionized water[34–35] and the deterioration of the long-term stability and performance of the CDI cells. The Faradaic reactions could be attributed to the reduction reactions at the cathode and the oxidation reaction at the anode[36–37]. Effect of the Faradaic reactions in a symmetric FB-CDI cell constructed from an AC powder with a polytetrafluoroethylene binder was investigated in a batch-mode[38]. Significant concentration of H_2O_2 was detected at the cathode during the desalination process (charging process) due to the reducing reaction of O_2 in electric consumption at the cathode (Fig. 18). The occurrence of H_2O_2 may well contribute to the fluctuation in pH of deionized water. While the occurrence of Faradaic reactions at the electrodes may contribute to deteriorate the stability and performance of carbon electrodes, and the presence of H_2O_2 might be also able to contribute the disinfection or the degradation of trace contaminants in the water.

N-doped carbon derived from ethylendiaminetetraacetic acid (EDTA, $C_{10}H_{14}N_2Na_2O_8$) by carbonization at 700, 750 and 800 °C for 2 h in Ar flow, washing by 0.5 mol/L HCl and deionized water[39]. The resultant carbons were mesoporous (S_{BET} of 257-596 m^2/g with V_{total} of 0.153-0.457 cm^3/g including V_{micro} of 0.076-0.185 cm^3/g) and have N-content of 9.1 at%-6.9 at% mainly at the pyridinic configuration. The CDI performances of the resultant carbons were studied by assembling a symmetric FB-cell with 5 mmol/L SAC NaCl solution in comparison with a commercial AC. The inlet solution was purged either with N_2 (de-aerated condition) to avoid the Faradaic effect of the dissolved oxygen on the electrode deterioration or with O_2 (aerated condition) to mimic the real practical desalination process. The dependences of SAC on applied voltage are shown in a flow of NaCl N_2-purged and O_2-purged solutions in Fig. 19a and b, respectively. In a de-aerated condition (Fig. 19a), SAC of the N-doped carbons becomes higher with increasing carbonization temperature and increases with increasing voltage applied, while that of the AC decreases above the voltage of 1.4 V. In an aerated condition (Fig. 19b), the increase in SAC for AC is more marked. On SAR the same tendencies in its changes with carbonization temperature and applied voltage were observed in de-aerated and aerated conditions. These decreases in SAC and SAR at high voltages were supposed to be due to the deterioration

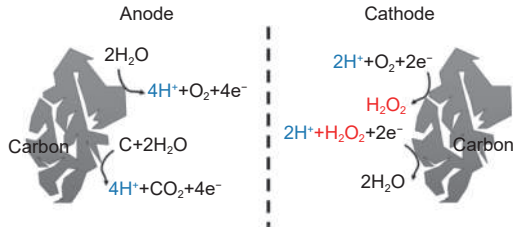

Fig. 18 Faradaic reactions at the carbon electrodes during water desalination. Reprinted with permission from Ref.[38]. Copyright (2016) by American Chemical Society

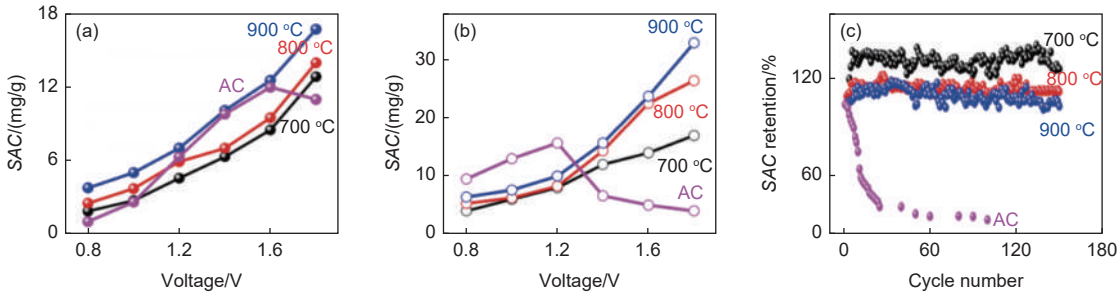

Fig. 19 CDI performance of N-doped carbons derived from EDTA by carbonization at 700, 750 and 800 °C in comparison with a commercial AC: dependences of SAC on the voltage applied in a flow of 5 mmol/L NaCl solution (a) in a de-aerated condition and (b) in an aerated condition, and cycle performance in an aerated condition. Reprinted with permission from Ref.[39]. Copyright (2021) by Elsevier

of carbon electrode by Faradaic reaction on the electrode surface. It is observed more markedly in the charge-discharge cycling, as shown the SAC retentions in an aerated condition in Fig. 19c, the deterioration of AC electrode occurs even at the beginning of the desalination/regeneration cycling. In contrast, the EDTA-derived carbons exhibited almost perfect cycling performances up to 150 cycles, the carbons obtained at 700 and 750 °C deliver higher SAC retentions (135% and 115%, respectively) than that of the carbon obtained at 800 °C (110% retention), respectively, whereas SACs of the 1st cycle for the former two are smaller than that of the latter (Fig. 19b). In de-aerated condition, similar cycle performances were observed on both carbons (the EDTA-derived carbons and the AC). An excessively high N-content up to 9 at% of the resultant carbons may result in the inhibition of carbon oxidation, associated with the improvement of the wettability and conductivity of the electrode carbons.

A biochar prepared from waste coconut shells at 550 °C for 2 h was activated with KOH in KOH/char mass ratio of 2 at 675 °C for 4 h (activated biochar AB), and then loaded MnO_2 nanoparticles by following 3 processes[40]: (1) mixing AB with $Mn(Ac)_2$ in HNO_3 solution at 60 °C (direct process), (2) mixing AB with $Mn(NO_3)_2$ in HNO_3 solution (indirect process) and (3) pre-treating biochar by HNO_3 at 120 °C and then mixed with $Mn(Ac)_2$ in HNO_3 solution (acid-assisted grafting oxidation (AGO) process). The activated biochar AB itself possessed S_{BET} of 486 m^2/g including S_{micro} of 98.5 m^2/g, while the carbon obtained through indirect process has S_{BET} of 304 m^2/g including S_{micro} of 54.7 m^2/g (higher than those of other 2 carbons obtained through direct and AGO processes). In Fig. 20a, electrosorption-desorption kinetics in 100 mg/L NaCl solution applying the potential of 1.2 and 0 V are compared on the pristine AB, MnO_2/AB composites prepared by the direct, indirect and AGO processes, revealing that MnO_2-incorporation is effective to enhance NaCl removal, particularly the MnO_2/AB composite obtained by the indirect process. In Fig. 20b, CV curve of the composite obtained through the indirect process is shown by dividing the capacitive contribution of 70.6%, ~30% Faradaic contribution. Total CDI performances of the MnO_2/AB composites were composed of relatively high capacitive contribution of ~70%.

Porous carbons derived from Zn-based zeolitic-imidazolate frameworks (ZIFs) with different ligands (ligand: mIm, eIm, 4abIm and Im) by carbonization at 1 000 °C for 1 h were applied to the electrodes of M-CDI cell with commercial anion-and cation-exchange membrane[41]. White ZIF powders were heated at 1 000 °C for 1 h in Ar flow and then naturally cooled down to 900 °C. On the cooling process, Ar gas was changed to NH_3 with a flow rate of 50 mL/min in the temperature range of 900 to 500 °C to obtain black

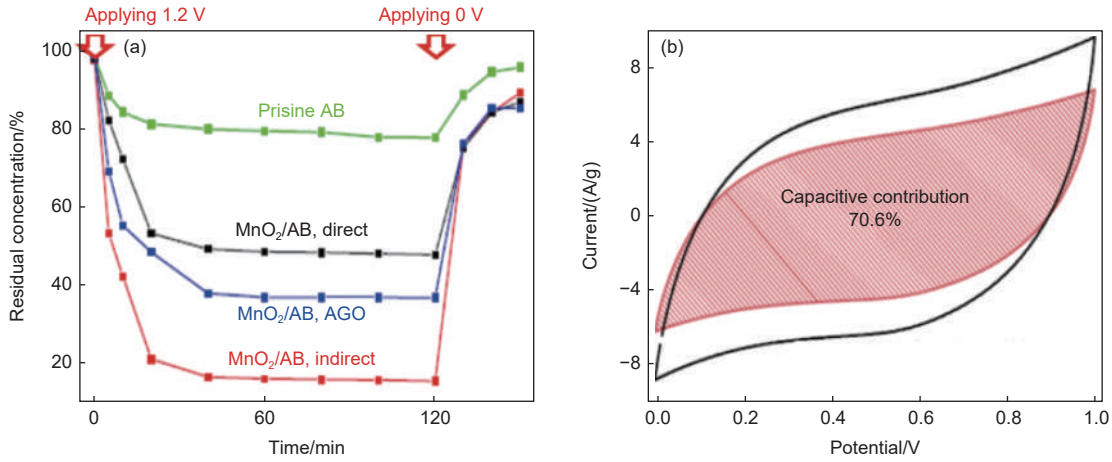

Fig. 20　CDI performance of the MnO_2/carbon composites: (a) adsorption-desorption kinetics in 100 mg/L NaCl solution by applying the potential of 1.2 and 0 V and (b) CV curve on the MnO_2/AB composite obtained through indirect process. Reprinted with permission from Ref.[40]. Copyright (2020) by Elsevier

powder of ZIF-derived carbons. S_{BET} of the resultant carbons was measured as 763, 380, 643 and 310 m^2/g for ZIFs with the ligands of mIm, eIm, 4abIm and Im, respectively. The carbon derived using 4abIm-ligands delivered the highest SAC for NaCl of 14.19 mg/g, greater than 13.33 mg/g of that derived using mIm-ligand and 6-9 mg/g of those derived using eIm- and Im-ligands.

2.4 Comparison between CDI cells

2.4.1 M-CDI cell

The Faradaic reactions occurring in batch-mode CDI cells, FB- and M-CDI cells, were compared by measuring the variations of H_2O_2 concentration, dissolved oxygen (DO) concentration, pH, conductivity of the deionized water under different charging voltages[42]. The CDI cells constructed using a commercial ACC (10 cm×10 cm with 300 μm thickness) having S_{BET} of 1 101 m^2/g at 2 electrodes (symmetric FB-cell) and using ion-exchange membranes with only AEM (AEM-CDI-cell), with only CEM (CEM-CDI-cell) and both AEM and CEM (M-CDI-cell). In Fig. 21a-d, the time changes in H_2O_2 concentration of the deionized water by applying different voltages (0.9, 1.2 and 1.5 V) for 4 CDI cells. In the FB- and AEM-cells, H_2O_2 concentration increases rapidly and then decreases during desalination (charging) process, which corresponds to the Faradaic reactions at the cathode, as illustrated in Fig. 18. In the regeneration (discharging) process, it decreases gradually with increasing time under 0 V. In the AEM-cell, higher maximum H_2O_2 concentration is attained at a shorter time during the desalination process than in the FB-cell, along with a higher H_2O_2 concentration at the end of desalination. In the M- and CEM-cells, on the contrary, the formation of H_2O_2 is strongly depressed. The time profiles in DO concentration in the deionized water in these CDI cells showed good correspondence to those of the time profiles of H_2O_2 concentration (Fig. 21) in respective cell. They are very similar in the FB- and AEM-cells, quickly decreasing with time in the charging process and slightly increases in the discharge process, and almost no change in both charging and discharging processes. The experimental result can be summarized that a marked increase and following gradual decrease in H_2O_2 concentration in FB- and AEM-cells, which corresponds to the Faradaic reactions at the electrodes to form and to consume H_2O_2 shown in Fig. 18. In contrast, a negligibly small generation of H_2O_2 in M- and CEM-cells are observed.

Polyglycerol powder prepared from a crude glycerol (a residual viscous liquid produced as a byproduct of the biodiesel process) was carbonized at 600 °C for 1 h in N_2 flow, activated at 850 °C for 1.5 h in N_2 flow after mixing with KOH powder in KOH/char mass ratio of 4 and then washed by 0.5 mol/L HCl and deionized water at 60 °C (Polyglycerol-derived activated carbon, PGAC)[43]. The PGAC exhibited S_{BET} of 1 684 m^2/g with V_{total} of 0.95 cm^3/g including V_{micro} and V_{meso} of 0.45 and 0.50 cm^3/g, respectively. The CDI performances of the PGAC was compared by construction of the symmetric and asymmetric FB-cells and two kinds of M-CDI cells, *i.e.*, using both AEM and CEM, and only CEM. An asymmetric FB-cell was constructed by using PGAC and HNO_3-treated PGAC at the positive and negative electrodes, respectively. The performances in 4 cells applying different voltages are compared by showing SAC, CE and energy consumption in Table 5. The M-

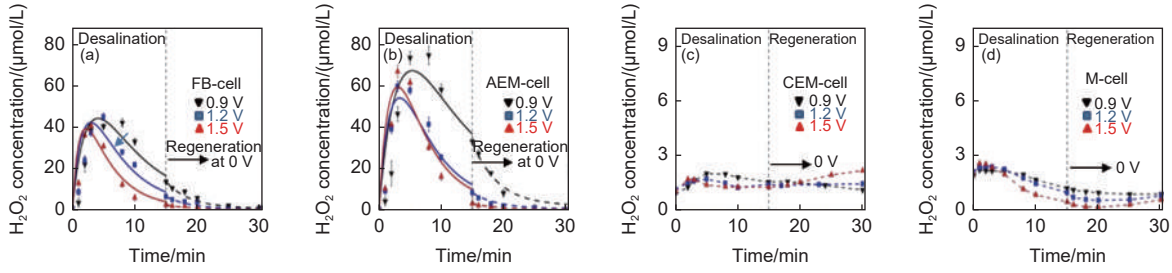

Fig. 21 Changes in H_2O_2 concentration in the effluent during charging at different voltages (0.9, 1.2 and 1.5 V) and discharging (0 V) in different type CDI cells: (a) symmetric FB-CDI cell, (b) AEM-CDI cell, (c) CEM-CDI cell, and (d) M-CDI-cell. Reprinted with permission from Ref.[42]. Copyright (2017) by Elsevier

Table 5　Desalination performance (SAC, CE and energy consumption) of the CDI cells with different configuration using the polygrycerol-derived activated carbon (PGAC) as the electrode material. Reprinted with permission from Ref. [43]. Copyright (2022) by Elsevier

Electrode configuration		Ion-exchange membrane	Cell voltage applied/V	*SAC*/(mg/g)	*CE*/%	Energy consumption/(J/mg)
FB-cell	Symmetric		1.1	10.8	65.4	2.8
			1.2	14.2	62.9	3.1
			1.4	13.7	51.2	4.6
	Asymmetric *		1.2	11.5	88.4	2.2
M-CDI		AEM and CEM	1.2	17.6	97.9	2.0
			1.4	23.4	102.9	2.3
			1.6	27.1	102.2	2.6
		CEM	1.2	16.8	98.9	2.0
			1.4	10.8	81.6	2.8

Note: *PGAC at the positive electrode and HNO_3-treated PGAC at the negative electrodes.

cell using both AEM and CEM delivered the highest performances, SAC of 27.1 mg/g, CE of about 100% at the cell voltage of 1.6 V. It also exhibited a stable desalination/regeneration cycle over the 50th cycle.

CDI performances of the conventional M-cell using both AEM and CEM placed on the front of carbon electrodes were compared to those of the cell with the electrodes composed of the membrane-coated carbon particles (individually-coated electrode cell, ICE-cell)[44]. A slurry of a commercial AC with a styrene-butadiene rubber binder was uniformly casted onto a graphite paper to a thickness of 350 μm and then coated by either AEM or CEM *via* respective NMP solution (10%, mass fraction), the resultant electrodes being used to construct CDI cell. The conventional M-CDI cell was assembled by placing commercial AEM and CEM in the front of the AC positive and negative electrodes, respectively. The ICE-cell delivered the SAC of 24.4 mg/g with CE of 89.4%, whereas the M-cell exhibited the SAC of 17.4 mg/g with CE of 88.3% at the voltage of 1.1 V. The results were explained by the suppression of Faradaic reaction on the carbon surface.

M-CDI cell was composed from single-wall carbon nanotubes (SWCNTs) formed using PTFE binder into the size of 70 mm×140 mm×0.3 mm and compared with the symmetric FB-CDI cell composed from the same SWCNT electrodes[45]. Fig. 22a shows the change in conductivity of the effluent solution after passing through the gap between two electrodes. The conductivity of the effluent after passing the cell at 1.2 V decreases rapidly from the initial conductivity of about 100 to about 0 μS/cm by M-CDI cell, but it decreases gradually down to about 40 μS/cm by FB-

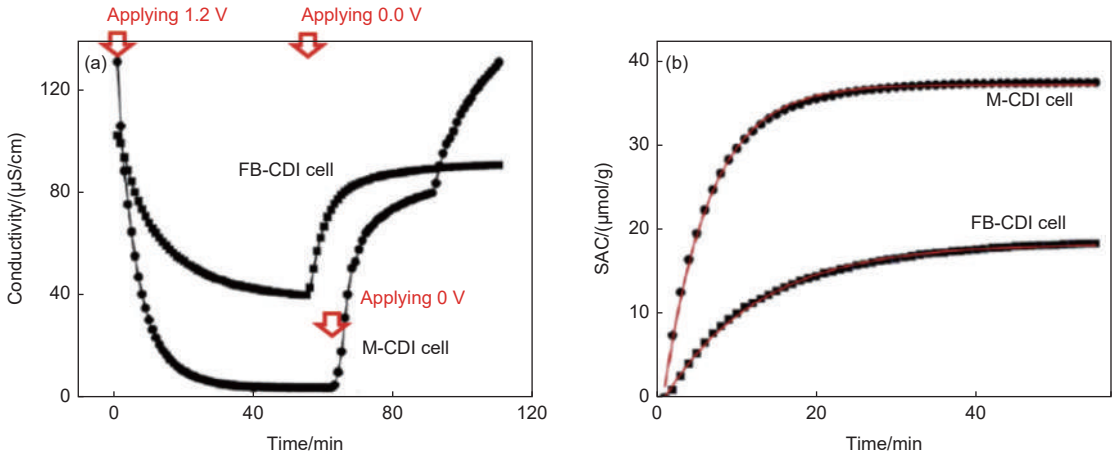

Fig. 22　Performance of M-CDI cell using SWCNT electrodes in FB-CDI using the same CNT electrodes: (a) conductivity change with time and (b) change in SAC with time. Conductivity of the initial solution is around 100 μS/cm and the voltage applied is 1.2 V.
Reprinted with permission from Ref.[45]. Copyright (2011) by Elsevier

CDI cell, suggesting a marked difference in SAC between 2 cells. The salt removal efficiency of M-CDI cell reached 97% but that of FB-CDI cell was about 60%, revealing that the presence of the ion-exchange membrane in the M-CDI cell is very beneficial for electrosorption of a salt ion by broking the counter-ions and so the salt removal efficiency by M-CDI cell is less affected by the presence of counter-ions. As shown the adsorption kinetics of these 2 cells at an applied voltage of 1.2 V in Fig. 22b, the SAR is much faster in the M-CDI cell than in the FB-CDI cell, which could be simulated by pseudo-first-order adsorption formula. As shown in Fig. 22a, the electrodes of M-CDI cell are almost completely regenerated by shutdown the electrode voltage through the desorption of ions, whereas those of FB-CDI cell cannot be completely regenerated due to the physical adsorption of counter-ions. In M-CDI cell, the desorption occurs in two steps: desorption is slowdown probably due to counter-ion effect at the surface of ion-exchange membrane and then accelerated again to complete desorption because no counter ions are at carbon electrode. The ion removal (desalination) and ion release (electrode regeneration) profiles for M-CDI cell were discussed by taking the stagnant diffusion layers in the front of the membranes[46].

M-CDI cell was constructed from a commercial ACC (thickness of 0.6 mm, S_{BET} of 1 117 m^2/g) and CEM and AEM with the thickness of 0.15 mm with 1×10^{-4} NaCl aqueous solution, and compared with the FB-CDI cell constructed from the same materials[47]. Salt removal capability of the M-CDI cell is higher than that of FB-CDI cell and the regeneration time is shorter in M-CDI than in FB-CDI (Fig. 23a). Changes in energy consumption (Wh/L) and salt removal percentage (%) with flow rate of salt solution and applied DC voltage are shown on the M-CDI cell in Fig. 23b and c, respectively. The salt removal percentage decreases as the flow rate increases but increases as the DC voltage increases. A marked decrease in the salt removal with the flow rate change from 40 to 60 mL/min. The electrical energy consumption also decreases with the increase in flow rate and increases with the increase in DC voltage. The M-CDI cell delivered the highest salt removal percentage of 62%, while the FB-CDI cell delivered only 24%.

Rode-shaped graphite electrode for CDI cell was coated by a porous carbon layer, of which a pair worked as the negative and positive electrodes in CDI cell[48]. In practice, the 7 pairs of these rod-shaped electrode positioned about 0.5 mm apart (FB-CDI cell) were dipped into a flow of NaCl aqueous solution. For comparison, another 7 pairs, of which the positive electrode was covered by ion-exchange membrane (M-CDI cell) were also prepared. In Fig. 24a and b, the kinetics for the removal of NaCl with the contact time up to 1 000 s and cycle performances up to the 5th cycle are compared for FB- and M-CDI cells, respectively. The M-CDI cell delivered a higher removal efficiency and a stable cyclability at a moderate potential of 1.2 and 1.6 V. The rod-shaped and even wire electrodes can be placed close together without requiring a spacer by filling the whole gap between the electrodes, and as the consequence can achieve saving space for the cell and reducing pressure drops of flowing water.

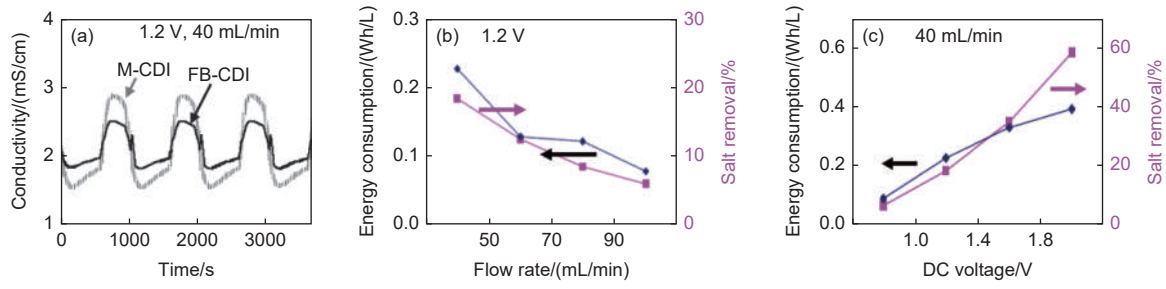

Fig. 23 Desalination performance of M-CDI using commercial ACC electrode with CEM and AEM: (a) desalination and regeneration profiles in comparison to FB-CDI, and (b) change in energy consumption and salt removal percentage with flow rate of salt solution and (c) those with DC voltage applied. Reprinted with permission from Ref.[47]. Copyright (2006) by Elsevier

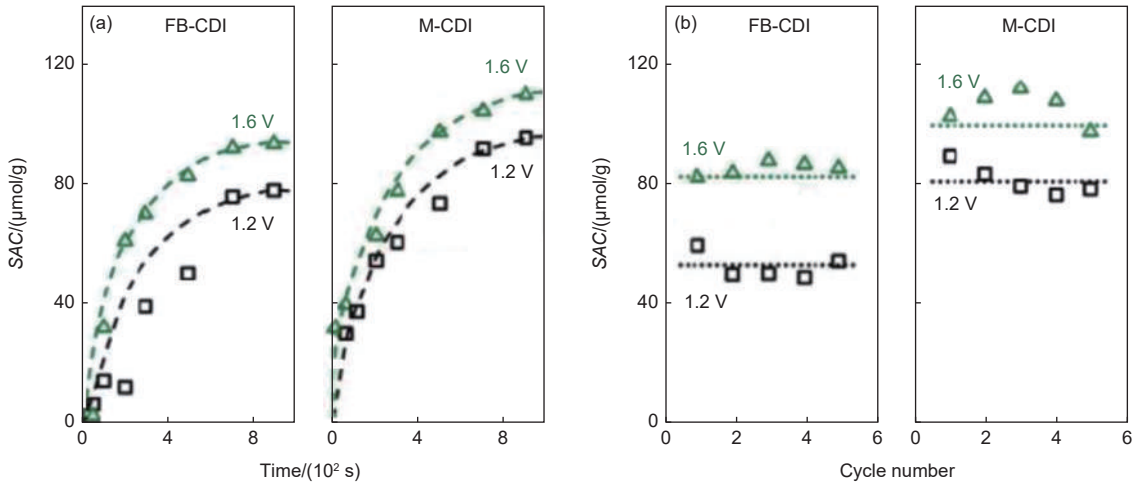

Fig. 24　CDI cells using rod-electrodes with or without ion-exchange membrane (FB-CDI and M-CDI): (a) adsorption kinetics and (b) cycle performance. Experimental points shown in the figures are average values of the values obtained by 12 cells. Reprinted with permission from Ref. [48]. Copyright (2012) by American Chemical Society

2.4.2　ETC-CDI cell

A symmetric two-electrode FTE-CDI cell was constructed using a carbon aerogel monolith having an interconnected pore network[49]. The aerogel was fabricated through the sol-gel polymerization of resorcinol with formaldehyde using acetic acid as a catalyst and following carbonization/activation at 950 °C for 2 h in a flow of CO_2, which exhibited a bimodal pore size distribution, 70% of the pore volume being attributed to macropores (about 0.7 and 2 μm diameters)[50]. The FTE-cell exhibited a very rapid desalination; the NaCl concentration dropped from 100 to 30 mmol/L within about 20 s by applying 1.5 V with sorption rate of nearly 1 mg/g·min[49]. PAN fiber webs prepared by electrospinning were treated with PVP in a different PVP/PAN weight ratios at 100 °C under hydrothermal conditions, were stabilized in air at 280 °C for 1 h and then carbonized at 800 °C for 0.5 h, followed by activation in CO_2 at 800 °C for 0.5 h[51]. The activated carbon nanofiber webs thus obtained using PVP/PAN weight ratio of 1 delivered the highest S_{BET} of 1 232 m^2/g with V_{total} of 0.786 cm^3/g including V_{micro} of 0.441 cm^3/g and the lowest bulk density of 0.71 g/cm^3. It also exhibited the high CDI performances, SAC of 6.51 mg/g and CE of 32.5%, while the web prepared the same procedures without addition of PVP delivered a little larger SAC of 7.61 mg/g but smaller CE of 23.7%.

2.4.3　FB-FTE-CDI cell

Two CDI cells, symmetric FB- and FTE-cells were constructed from a commercial carbon nanofoam (NF) and an ACC, and compared their CDI performances in NaCl solution[52]. Ti metal (thickness of 0.127 mm) was used as the current collector, and the carbon electrodes were separated by a hydrophilic PTFE porous membrane having pores of 5 μm size (thickness of 85 μm). The FB-CDI cell consists of a rectangular compartment with the size of 29.5 mm× 58.9 mm×2 mm, while the FTE-CDI cell consists of a circular flow chamber with 47 mm in diameter. In Table 6, the physical characteristics of the carbons used as the electrodes in the cells are summarized for NF and ACC, together with another commercial ACC (K-ACC). In Fig. 25a and b, the SAR is plotted

Table 6　Commercial carbon nanofoam (NF), activated carbon cloth (ACC) and another ACC (K-ACC) used for construction of symmetric FB- CDI-cell and FTE-CDI-cells. Reprinted with permission from Ref. [52]. Copyright (2018) by Elsevier

Carbon	Thickness/μm	S_{BET}/(m^2/g)	V_{micro}/(cm^3/g)	Capacitance/(F/g)	Resistance/(Ω/sq)	O-content/at%	SEM features
NF	210	705	0.27	100	0.4	2.1	10-100 cracks, <10 nm pores
ACC	500	2980	0.44	110	3.9	6.6	13 μm-diameter fibers, <300 nm pores
K-ACC	800	1913	0.31	80	3.3	4.8	14 μm-diameter fibers, <300 nm pores

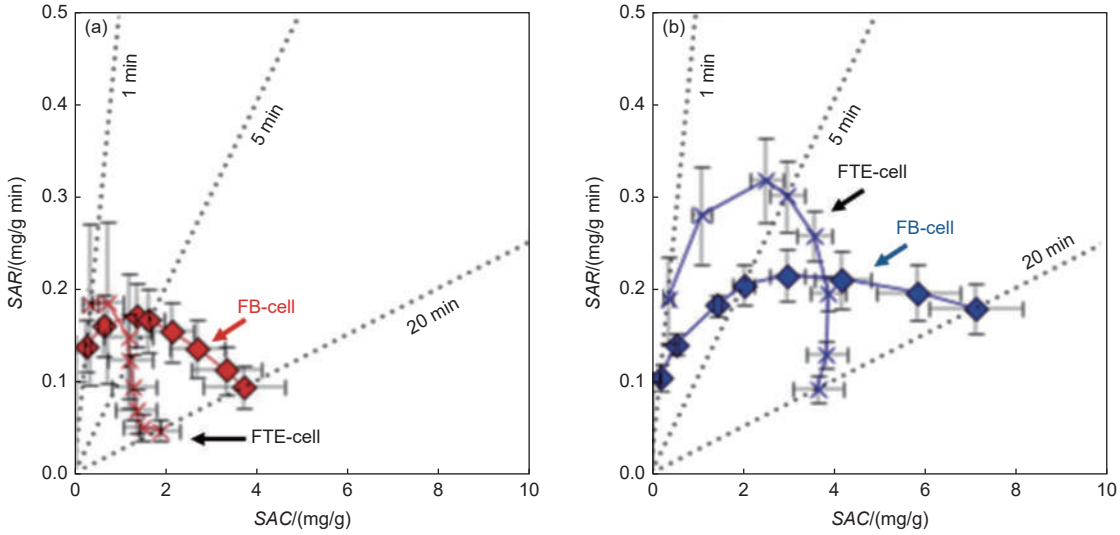

Fig. 25 Comparison in the CDI performances between FB-CDI cell and FTE-CDI cell using carbon electrodes of (a) a carbon nanofoam and (b) an ACC. Reprinted with permission from Ref. [52]. Copyright (2018) by Elsevier

against the SAC measured on the FB- and FTE-cells for the electrode materials, NF and ACC, respectively. The maximum salt removal is achieved at 3.72 mg/g for NF and 7.13 mg/g for ACC at the contact time of 20 min by the FB-cell, while it is 1.87 mg/g for NF at 20 min and 3.90 mg/g at 10 min for ACC by FTE-cell (Fig 25a and b, respectively), the SAC of ACC being about two times larger than that of NF in both cells. On the SAR, ACC delivers also much higher maximum rate than NF and is higher in the FTE-cell than in the FB-cell, 0.32 mg/g·min at 4 min and 0.21 mg/g·min at 7 min, although the highest SAR of 0.18 mg/g·min at 2 min for NF in both cells. The salt removal performances in both FB- and FTE-cells of another ACC (K-ACC) are almost comparable with the ACC, although S_{BET} is much larger than ACC, as shown in Table 6. The SAC of the ACC decreased with desalination-regeneration cycles, decreasing by 57% in the FB-cell and by 77% in the FTE-cell after 120 cycles. The SAC decrease was faster in the FTE-cell than the FB-cell. This depression in SAC was supposed to be due to the oxidation of carbon electrode during salt removal processes. O-content of the NF increased from 2.1 at% to 9.2 at% and 11 at% after the use for 48 h in the FB-cell, and that of the ACC increased from 6.6 at% to 13 at% and 19 at% in the FTE-cell.

Desalination performances of the FTE-CDI cell were studied by changing the flow modes of the saline water, *i.e.*, a flow from anode to cathode (forward flow mode) and a reverse flow from cathode to anode (reverse flow mode) in comparison with the FB-CDI cell[53]. CDI cells were constructed using a commercial ACC having S_{BET} of 1 101 m^2/g as elec-

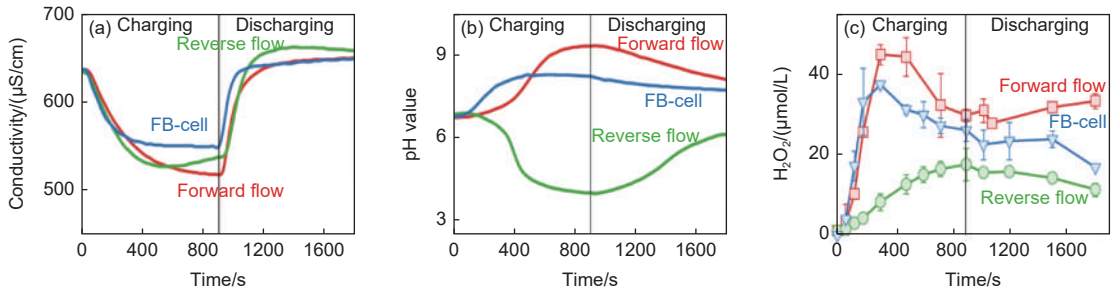

Fig. 26 Change in conductivity, pH and H_2O_2 concentration of the effluent passed through the cells, FTE-CDI cell with a forward flow, that with a reverse flow and symmetric FB-CDI cell at an applied voltage of 1.2 V with time during charging (desalination process) and discharge (regeneration process): (a) conductivity, (b) pH and (c) H_2O_2 concentration. Reprinted with permission from Ref.[53]. Copyright (2019) by Elsevier

trode material. In Fig. 26a-c, the changes in conductivity, pH value and H_2O_2 concentration of the effluent by applying 1.2 V are shown for 3 CDI cells in charging (desalination process) and discharging processes (regeneration prosses). The conductivity of the effluent decreases sharply and then reaches a relatively steady conductivity within 15 min. As shown in Fig. 26a, FTE-cell with forward flow mode achieved the lowest conductivity, which corresponds to SAC of 11.1 mg/g, being higher than those of FB- and FTE-cell with reverse flow mode, 8.2 and 10.2 mg/g, respectively. The pH value of the effluent in the FTE-cells fluctuates more severely than in the case of the FB-cell (Fig. 26b). pH value increases to a peak value of 9.3 during the charging and then tends to decrease back to about 8.0 in the discharging process in the FTE-cell with forward flow mode. When operated in reverse flow mode, the pH value decreased rapidly to about 4 and then recovered gradually, looks like to be reversed the change in the forward mode. In the FB-cell, the pH of the effluent changed only slightly. H_2O_2 concentration of the effluent increases rapidly at the beginning of the charging process but then gradually decreases in FTE-cell with forward flow mode and FB-cell, H_2O_2 concentration reaching 45 and 37.5 mmol/L, respectively. In the FTE-cell with reverse flow mode, H_2O_2 concentration exhibits a relatively slower increase and achieves a peak value of 17.6 mmol/L at the end of the charging process. The changes in pH and H_2O_2 concentration in the effluent was discussed by relating to Faradaic reactions at the surfaces of the carbons at the negative and positive electrodes.

2.5 Modification of CDI cells

2.5.1 M-CDI cell

Prussian blue (PB, $Fe_4[Fe(CN)_6]_3$) and its analogues (PBAs) have an open framework structure that can adsorb and store almost all alkali metals and even multivalent metals, such as Na, Mg, Ca, Zn and Al. PBAs are represented as $A_xM_{Ay}[M_B(CN)_6]_z{\cdot}nH_2O$, where M_A and M_B are usually Mn, Fe, Co, Ni, Cu or Zn, and A is usually Li, Na or K. The composites of ACC with PBAs were proposed to enhance CDI performances of FTE-cell[54–55]. The deposition of a PBA using Co on ACC showed a stable CDI performance, reaching a SAC of 14.47 mg/g at 1.0 V, accompanied by a low energy consumption of 389 Wh/m^3[54].

A three-electrode cell (3-CDI cell) was constructed by combining the concepts of FB- and FTE-cells, as shown as an inset of Fig. 27b[56]. The carbon for the cell electrodes was composed from commercially available ACCs (6 cm×6 cm size with 2 mm thickness) either as-received (ACC) or its 1 mol/L HCl-treated (H-ACC) and both felts (ACC and H-ACC) delivered similar capacitances in 1 mol/L NaCl aqueous electrolyte. The salt adsorption kinetics in the asymmetric FB-cell (ACC/H-ACC) and 3-CDI cell (ACC/H-ACC/ACC) are shown in Fig. 27a and b, respectively, together with the schematic illustrations of each cell (insets). A higher SAC and faster SAR are realized in 3-CDI cell in comparison to the FB-cell with a asymmetric electrode configuration. An insertion of flow-through electrode (FTE) in a conventional symmetric FB-cell, *i.e.*, 3-CDI cell, was shown to

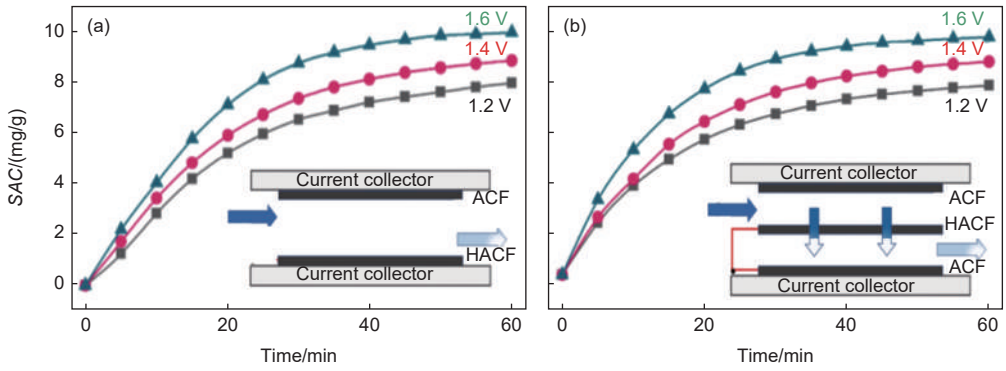

Fig. 27　Salt adsorption kinetics at different voltages (1.2-1.6 V) constructed from commercial activated carbon fiber felt (ACF) and HCl-treated ACF (HACF); (a) asymmetric FB-cell and (b) 3-CDI (inserted a flow-through electrode). Reprinted with permission from Ref. [56]. Copyright (2021) by Elsevier

be effective to achieve a higher CE, lower energy consumption, shorter desorption time and good cyclic stability. The insertion of more FTEs (4-CDI and 5-CDI cells) resulted in poorer long cycle stability.

FTE-cell using ACC electrode worked not only for the desalination of a brackish ground water collected from a well in Oman, which had pH value of 8.0 with TDS (total dissolved solids) of 2 500 mg/L, but also for the disinfection of the water[57]. The as-received water had the CFU (bacterial colony forming unit) of about 3.0×10^4, while the water after desalination process had about 70% smaller CFU.

2.5.2 FE-CDI cell

Flowing electrode CDI (FE-CDI) is receiving increasing attention due to its pseudo-infinite capacitive desalination, which is achieved by continuous regeneration of electrode carbon particles in the external reservoir. FE-CDI can also desalinate significantly higher salinity feeds than other CDI systems. A flowing electrode of a FE-CDI cell composed of a 0.1 mol/L NaCl aqueous solution containing 5% (mass fraction) AC particles with 8.8 μm size exhibited excellent removal efficiency more than 95% and a high SAR of 0.41 mg/min·cm from a brackish stream of an aqueous NaCl solution with a high concentration as 32.1 g/L, such as seawater[58–59].

The FE-CDI cell consists of the flowing electrode of the mixture of a 100-mesh AC (DARCO), chemically activated charcoal, and carbon black powders in a mass ratio of 8∶1∶1 suspended in 2 000 mg/L NaCl with an initial pH of around 7[60]. For investigation on the water softening, the brackish stream containing 2 000 mg/L NaCl and 150 mg/L $CaCl_2$ was used. The brackish water was passed through the space between AEM and CEM at different flow rates resulting in hydraulic retention times (HRT) (contact time) of 2.94, 1.47 and 0.98 min, respectively. The water desalination and softening were carried out in short-circuited closed-cycle (SCC) operation, as illustrated in Fig. 28a, and in the isolated closed-cycle (ICC) operation, as illustrated in Fig. 28b. In the former operation, the flowing-electrodes are mixed in a shared reservoir after leaving the CDI cell, resulting in charge neutralization of the carbon particles, in other words, the electrode regeneration can be achieved by continuously mixing with oppositely charged carbon electrode in the reservoir. In the latter operation, however, the positively and negatively charged flowing-electrode is individually recycled in their respective pipelines. As shown in Fig. 29a, SCC operation required much lower energy consumption than ICC, particularly low effluent conductivity (*i.e.*, low salinity) be able to achieve much lower energy consumption than ICC. In SCC operation conditions, average salt removal rate (ASRR) and energy-normalized removed salt (ENRS) do not depend on HRT, in other words, on the flow rate of the brackish water (Fig. 29b). In Fig. 29c, the voltage changes with elapsed time during SCC and ICC operations. After 4 800 s kept at the constant-current (charging step), the current was reversed for 2 400 s (discharge step). In SCC operation, the cell voltage re-

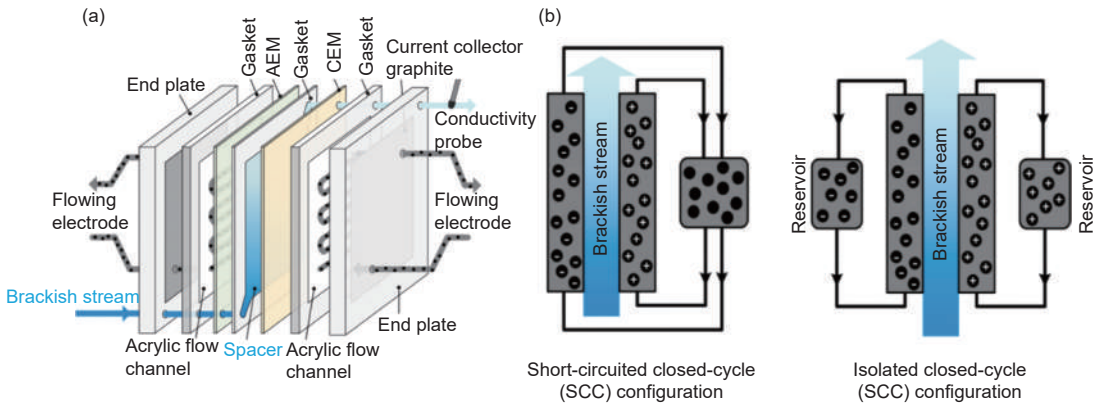

Fig. 28 Schematic representations of (a) the structure of the CDI cell and (b) short-circuited closed-cycle (SCC) and isolated closed-cycle (ICC) configuration of the system. Reprinted with permission from Ref. [60]. Copyright (2018) by American Chemical Society

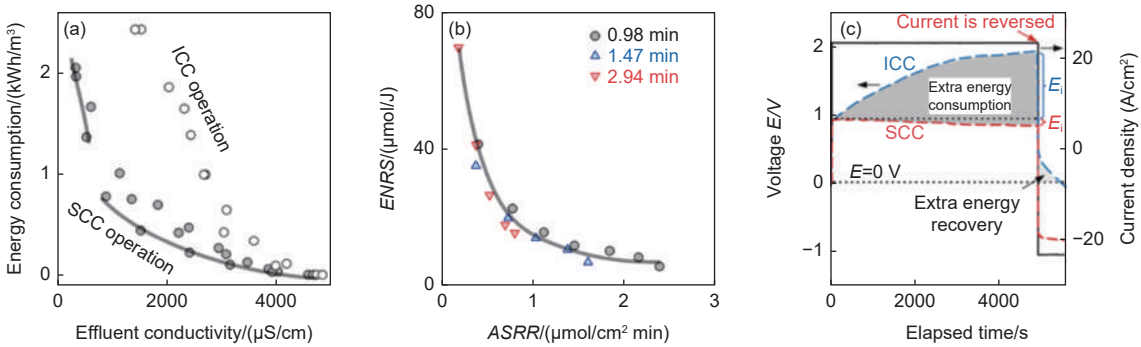

Fig. 29　FE-CDI cell for water desalination and softening by a mixture of commercial AC and carbon black as the flowing electrode: (a) energy comparison of SCC and ICC operations, (b) relation between average salt removal rate (*ASRR*) and energy-normalized removed salt (*ENRS*) in SCC operation at different HRT (different flow rate of brackish water), (c) voltage changes with elapsed time in ICC and SCC operations. Reprinted with permission from Ref. [60]. Copyright (2018) by American Chemical Society

mained stable at a little below 1.0 V with a slight decrease (E_i in Fig. 29c), which is most likely related to the increasing ion concentration in the flowing-electrodes. In contrast, the voltage in ICC operation increases gradually up to 1.92 V, resulting in an energy consumption of 0.39 kWh/m^3 in an excess of the energy consumption for SCC operation. While the anode and cathode are potentially isolated allowing for energy recovery during electrode regeneration, only about 0.012 kWh/m^3 (Fig. 29c). Divalent cation Ca^{2+} was selectively removed in comparison to monovalent Na^+ of which the selectivity became dominant when the FE-CDI cell was operated at a low current density and a low HRT. An extremely high water recovery rate of about 95% could be achieved when desalting a 1 000 mg/L NaCl brackish influent to a potable level of 150 mg/L by FE-CDI cell with SCC operation using a mixture of commercial carbon black and two ACs with S_{BET} of 920 and 1 050 m^2/g[61].

Effect of NaCl concentration in the flowing-electrode solution was studied on a FE-CDI cell with SCC operation mode[62]. Commercial AC spheres after purification were mixed with NaCl aqueous electrolyte solutions with different concentrations. The desalination of NaCl solution (brackish solution) with 35 g/L concentration was passed through the space in the FE-CDI cell at a flow rate of 3 mL/min, and the flow rate of the flowing-electrodes operated with SCC operation mode (Fig. 28b) was maintained constant at 25 mL/min. In Fig. 30, the relations of desalination efficiency to the current applied to the cell and NaCl concentration in the flowing electrode solutions after cyc-

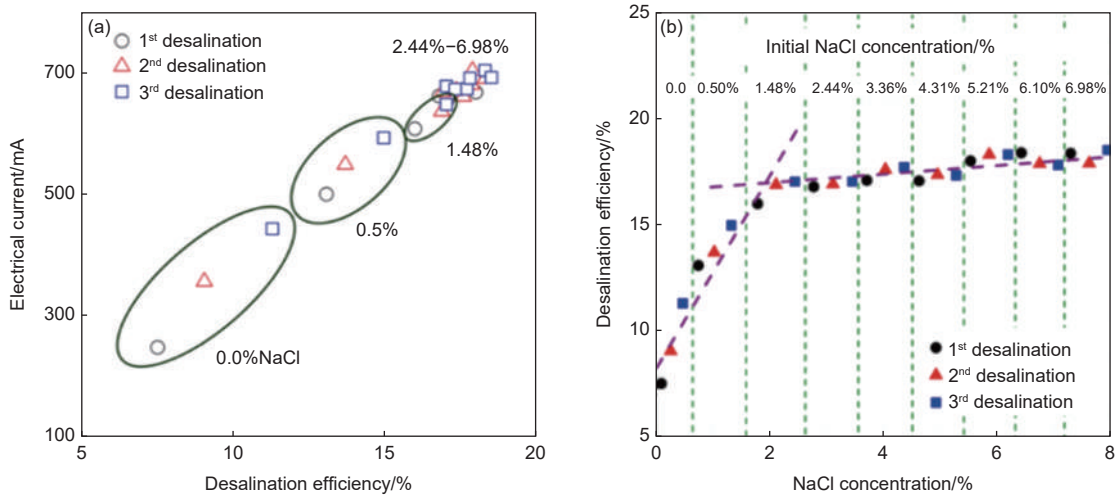

Fig. 30　Desalination performances of the FE-CDI cell with SCC operation: (a) the relation between desalination efficiency and electrical current with varying NaCl concentrations (0-6.98%) and (b) the relation between desalination efficiency and NaCl concentration in the flowing-electrode after 1st/2nd/3rd desalination processes. Reprinted with permission from Ref. [62]. Copyright (2016) by American Chemical Society

ling (1st to 3rd). As shown in Fig. 30a, the desalination efficiency is linearly related to the current applied, with the cycling of the flowing-electrode solution and with increasing in the initial NaCl concentration. The increase in desalination efficiency seems to be saturated at initial NaCl concentration above 2.44% (mass fraction). In Fig. 30b, therefore, desalination efficiency is plotted against the NaCl concentration of the flowing-electrode solution, demonstrating a marked increase in efficiency up to 2% (mass fraction) and a tendency to be saturated. The experimental results demonstrate that high desalination efficiency of more than 17% can be obtained by increasing NaCl concentration to more than 2.44% (mass fraction), while a high current as 700 mA is required. The performances of FE-CDI cell with SCC operation mode were studied on different types of the AEMs and CEMs[63]. The energy consumed during the desalination process in a FE-CDI cell using a mixture of AC with CNT as the flowing-electrode was recovered by a two-chamber device, where the adsorbed electrodes were discharged with constant current[64]. The addition of CNT in the flowing-electrode made the energy recovery ratio higher, about 7.5% without CNT and about 12% recovery with CNT-addition. Increased salt concentration of the electrolyte solution could decrease the energy consumption during desalination process and improve the energy recovery. The energy recovery ratio was promoted to 9.4% when the salt concentration of the electrolyte increased to 9.60 g/L. In FE-CDI cells, the concentration of the flowing-electrode carbons is limited to about 20% (mass fraction), resulting in a poor electronic conductivity (reported to be 0.1-1 mS/cm) mainly due to the transportation of electric charge through a discontinuous network of carbon particles. It is reasonably supposed that electronic conductivity of the flowing electrodes is governed by their concentration (weight percentage, CWP, %). In the reservoir, two suspensions of carbon electrodes came back from the positive and negative electrodes of the cell are continuously stirred using a mixer at 300 r/min in order to prevent carbon particle sedimentation and ensure a fairly uniform carbon concentration to maintain flowability (fluidized bed CDI-cell)[65]. In this fluidized bed CDI-cell, phenolic-resin-derived microporous AC spheres with the diameter of 125-250 μm were employed and carbon concentration in flowing-electrode slurry could be increased up to 35% with maintaining a sufficient flowability.

A FE-CDI cell consisted of a stack of the membrane-current collector (MCC), as illustrated in Fig. 31, was proposed (named as a gradient FE-CDI system) for enlarging the scale of desalination with improved performance and simplifying the device[66]. Under the optimal operating conditions for the system with four MCC units (content of electrode carbon of 10%, brackish water with 3 000 mg/L NaCl, cell voltage of 1.2 V, and productivity of 56.7 L/m^2·h), the ASRR of 1.07 μmol/cm^2 min and ENRS of 7.8 μmol/J were verified at long-term operation (over 56 h).

Coupling of a liquid membrane chamber (LMC) with a conventional FE-CDI cell with a flowing-electrode slurry containing 5% carbon (a mixture of AC with carbon black in 5∶1 by weight) was shown to be effective for the selective recovery of P and N (*i.e.*, urea) from fresh human urine[67]. The LMC consisted of two AEMs placed in parallel and sandwiched between the spacer chamber and the anode chamber. In charging process, negatively charged P ions (*i.e.*, HPO_4^{2-} and $H_2PO_4^-$) were captured by acidic extraction solutions (*e.g.*, HCl, HNO_3 and H_2SO_4) of the LMC, leading to the conversion of P ions to H_3PO_4, on the way to the anode of FE-CDI cell in SCC operation mode. Under the optimal operating conditions, satisfactory performance of P and N removal and desalination efficiency (91.1%) were obtained after 37.5 h of continuous operation.

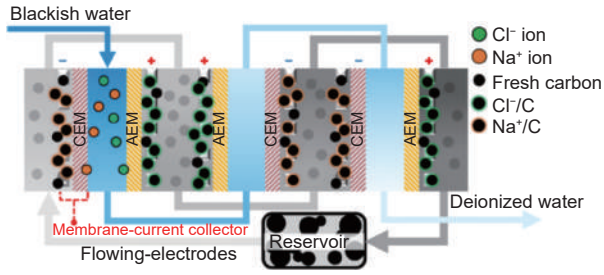

Fig. 31 Schematic representation of a gradient FE-CDI system in the gradient single cycle (GSC). Reprinted with permission from Ref. [66]. Copyright (2021) by American Chemical Society

2.6 New CDI cells

2.6.1 Inverted-CDI cell

An inverted capacitive deionization (inverted-CDI) cell configuration was proposed, in which desalination is mainly achieved by a spontaneously formed EDL at a modified surface of a carbon electrode without an external power supply, while an applied voltage from an external power source is used to desorb ions (Fig. 32a and b), respectively[68].

One-side of the electrode carbon (carbon cloth) was coated by a mixed slurry of bromomethylated poly-(2, 6-dimethyl-1, 4-phenylene oxide) (BPPO) with NMP through splaying to get BPPO-coated carbon cloth and followed by either sulfonation or amination, which were submitted to investigate CDI performances[69]. The sulfonation of the BPPO-coated carbon cloth was performed by immersing into 99% sulfuric acid for 20 min at room temperature and then transferred to 80%, 50% and 30% sulfuric acid solution for 1 min. The amination of the BPPO-coated carbon cloth was achieved by immersing into 25% trimethylamine (TMA) for 20 min. The CDI cells were constructed by coupling the pristine carbon cloth at two electrodes (symmetric FB-CDI cell), sulfonated and aminated BPPO-coated carbon cloths at the negative and positive electrode, respectively (inverted-CDI cell), and covering the pristine carbon cloth electrodes by commercial CEM and AEM (M-CDI cell). For these 3 CDI cells, CDI performances based on the data measured after 30 min operation are summarized in Table 7. The inverted-CDI cell exhibits a marked decrease in conductivity of the effluent, although the same initial conductivity is employed. The inverted-CDI cell delivers a little higher salt removal efficiency of 83% than the FB-CDI cell (79%), much higher efficiency than M-CDI cell, while it consumes much smaller power during 30 min operation, power consumption for the inverted-cell being smaller by one order of magnitude and that for M-CDI-cell smaller by two-orders from FB-CDI cell. These results demonstrate that the surface modifications, sulfonation and amination, of the BPPO-coated carbon cloths are very effective. The inverted-CD-cell exhibited a stable cycle performance with the regeneration of the electrodes by reducing the potential to zero.

2.6.2 Rocking-chair-CDI cell

New idea for CDI system of water desalination (named rocking-chair-CDI) was proposed[70]. The cell consists of a Nafion-coated AC electrode in channel A and in channel B, and these 2 channels are separated by an anion-exchange membrane (AEM) (Fig. 33). During the constant-current operation in the cell, the solution in channel A is concentrated by the released cations from the carbon electrode (positive) in channel A and by the anions transported through AEM from the solution in channel B whereas the solution in channel B is diluted due to electrochemical adsorption of cations by carbon electrode balancing with an-

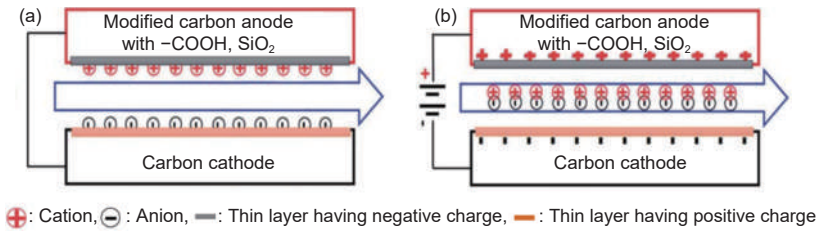

Fig. 32　Schematics of the inverted-CDI cell: (a) desalination process and (b) desorption (regeneration)[68]

Table 7　Comparison in salt removal efficiency, current, and power consumption for three CDI cells. Reprinted with permission from Ref.[69]. Copyright (2011) by Elsevier

Cells	Applied potential/V	Solution conductivity/(μS/cm)		Salt removal efficiency/%	Current after 30 min/mA	Power consumption/(mW/h)
		Initial	After 30 min			
FB-CDI cell	1.8	190.8	39.9	79.1	235.7	212.3
M-CDI cell	1.8	185.1	168.0	9.2	2.6	2.3
Inverted-CDI cell	1.8	188.9	31.5	83.4	25.6	23.1

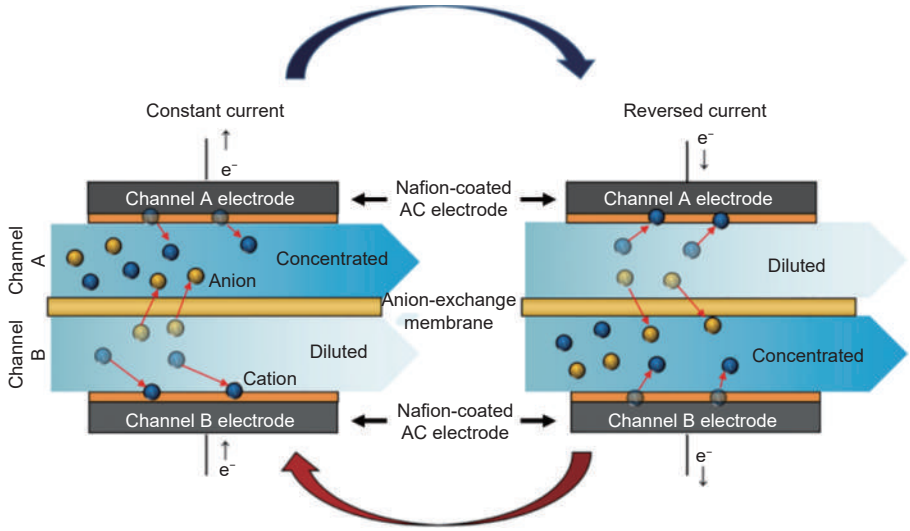

Fig. 33 Schematic illustration of the rocking-chair-CDI cell. Reprinted with permission from Ref.[70]. Copyright (2018) by American Chemical Society

ion diffusion to the solution in channel A through AEM. By reversing current, the solution in channel A is diluted and the solution in channel B is concentrated by the reverse movement of cations and anions. The carbon electrode was prepared by mixing and rolling a mixture of a commercial AC with acetylene black (conducting agent) and poly(tetrafluoroethylene) (binder) to a sheet with the thickness of 300 μm on graphite sheet (current collector), and then the surface of AC layer was coated by Nafion *via* drop-casting[70]. The rocking-chair-cell delivered high SAC of 44.6 mg/g and high ACR of about 0.05 mg/g·s, which was much higher than those of M-CDI cell. It also exhibited a marked cycle stability, at a constant-current operation with a current density of ±12.5 A/m^2 in 10 mmol/L NaCl solution the SAC and CE increasing gradually with cycling up to the 35th cycle.

3 Carbon materials for battery-type deionization cells

3.1 Cation-intercalated DI cell (Hybrid cell)

Water desalination with electrochemical process (Faradaic reaction) has been shown to be possible by battery-functionality of the electrodes, capturing metallic ions, mostly Na^+, in the crystalline lattice site of the electrode materials. The process of the ion-capturing is often called “intercalation”, even though it is different from the process for capturing Li^+ (*i.e.*, intercalation of Li^+ into interlayer space of graphite) at the negative electrode of lithium-ion rechargeable batteries, while being similar to re-capturing to vacant lattice site, formed after charging of the battery, in $LiCoO_2$ crystal at the positive electrode. Therefore, the electrode materials for battery-type cells for water desalination have been constructed using inorganic crystals, such as $Na_{2-x}Mn_5O_{10}$, $Na_4Mn_9O_{18}$, λ-MnO_2, $NaCuFe(CN)_6$, etc. at the electrodes.

A cell was assembled by a commercial AC with an AEM at the positive electrode with a synthesized sodium manganese oxide ($Na_4Mn_9O_{18}$, NMO) at the negative electrode[71]. The NMO electrode was pretreated at 0.8 V for 60 min to extract Na^+ (to form $Na_{4-x}Mn_9O_{18}$) before the desalination performance test. The CDI cell, Na^+ are captured by the Faradaic reaction at the Na-extracted NMO electrode (negative electrode), and Cl^- are adsorbed on the surface of the AC positive electrode by principally electric double-layer (EDL) formation during the desalination process. Principal desalination mechanism in this deionization cell (DI-cell) is the Faradaic reaction at the negative electrode and the EDL formation at the positive electrode, may classified into a hybrid cell. This hybrid cell exhibited a salt removal capacity of 31.2 mg/g, almost double from a symmetric FB-CDI cell composed from AC (13.5 mg/g). It gave a rapid ion removal rate (0.072 mg/g·s) and an excellent stability.

3.2 Redox-flow deionization cell (DI cells)

A symmetric cell composed from $Na_{0.44}MnO_2$-based electrodes that were separated by an AEM was proposed for Na-ion desalination[72]. From the gap separated by AEM, the desalinated effluent on one side and the concentrated effluent on another side were obtained separately, in one side Na^+ was desalinated by accommodation (intercalation) into the lattice sites in $Na_{0.44}MnO_2$ and Cl^- (redox reaction) was expelled to another side of the gap through AEM to keep charge balance in the electrolyte, resulting in the desalinated effluent, while the concentrated effluent was obtained in another side.

Redox-mediated deionization (redox-flow deionization cell, redox-flow DI cell) was proposed for water desalination[73]. The desalination cell is composed of individual two channels, one for feeding of brackish water and another for circulation of supporting electrolytes between positive and negative electrodes, similar to the cell shown in Fig. 34. Each channel is completely separated from the feeding water by CEM and AEM. For the electrodes, ACCs, either as-received or after N-doping, were employed and were placed next to the side channels[74]. N-doping was carried out by heat-treating a mixture of ACC with urea at 150 °C for 2 h and successively at 300 °C for more 2 h (N-ACC), its N-content being 3 at%. The circulating a feed stream of 10 mmol/L NaCl solution (500 mL) at feed channel and redox stream of a 100 mmol/L NaCl solution containing a 100 mmol/L $Na_3Fe(CN)_6/Na_4Fe(CN)_6$ solution (100 mL).

Redox-DI does not require a discharging cycle to regenerate the electrodes. Moreover, the desalination performance of the redox-DI cell was largely dependent on the electrodes. This can be confirmed by the noticeable decrease in the conductivity profile and high operational current flow (left inset of panel A) for N-ACC compared to ACC. In particular, the conductivity of effluent was gradually decreased (*i.e.*, unsteady-state condition) as the operational time was increased (Fig. 35a). With the accumulated salt in the side channel, the ionic strength at the side channels was increased, resulting in a better environment for redox reaction on N-ACC in terms of capacitive and electrocatalytic properties (Fig. 35b).

4 Co-generation of electric power in CDI process

A CDI cell was demonstrated to apply for the extraction of energy from the water solutions with dif-

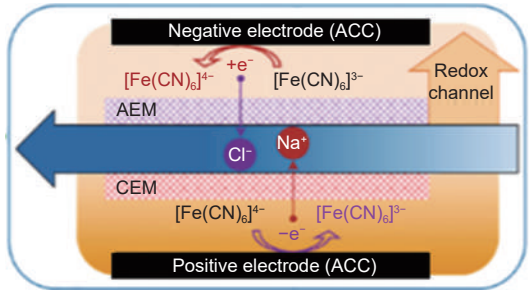

Fig. 34　Schematic illustration of a redox-flow DI cell. Reprinted with permission from Ref.[73]. Copyright (2022) by Elsevier

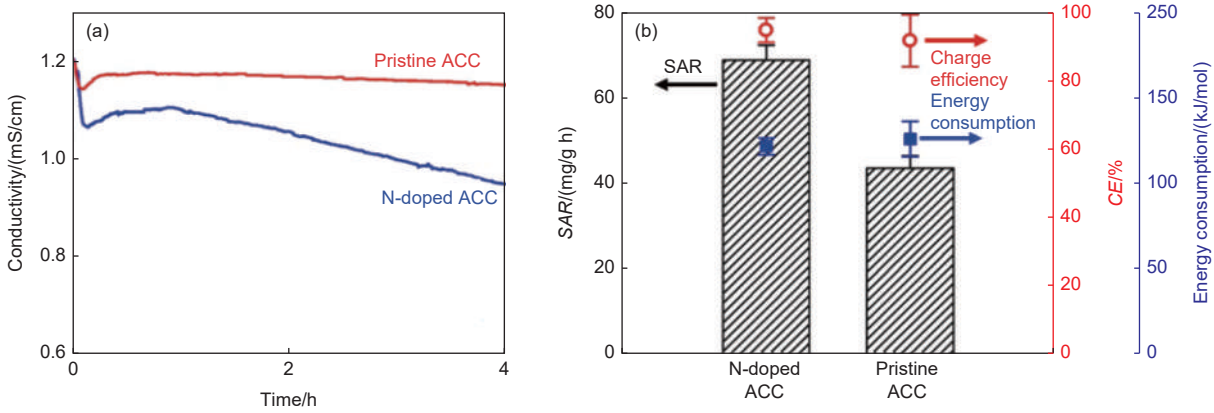

Fig. 35　Performance of the redox-flow DI cell using electrodes of a commercial (pristine) ACC and N-doped ACC: (a) conductivity profiles of the effluents when the pristine and N-doped ACCs were used, and (b) the desalination performance the cells using the pristine and N-doped ACCs. Reprinted with permission from Ref. [74]. Copyright (2021) by Elsevier

ferent salinity, such as river water and sea water[75]. The cell consisted of a commercial AC having S_{BET} of 650 m^2/g with V_{total} of 0.95 cm^3/g, apparent density of 0.38 g/cm^3 and resistivity of 0.9 Ω/cm. In Fig. 36a and b, the process in 4 phases A to D in one cycle and corresponding potential *vs.* charge curves are schematically shown in Fig. 36a and b, respectively, with which energy extraction of about 5 μJ was achieved by a cycle. The cell is filled with salt water with high concentration (high salinity solution) and is charged to a voltage ϕ_{charge} of about 300 mV (phase A), and then it is flushed with a fresh water (low salinity water) under open circuit (voltage increases up to ϕ_B of about 333 mV) (phase B). A following discharging of the cell makes the voltage $\phi_{discharge}$ decrease down to about 300 mV (phase C) and then the circuit is open in a flow of salted water associating with the decrease in voltage down to ϕ_D of about 274 mV (phase D). In this cycle from phase A to D, the cell can extract an energy of about 5 μJ from the salinity difference per one cycle.

A novel electrochemical cell was proposed to extract energy from the difference in concentration of two solutions and to store it as chemical energy inside the crystal structure of electrode materials and named a "mixing entropy battery" or "battery-functionated CDI cell"[76]. In this battery, the electrolyte is NaCl solution and two different electrodes are selected, an anionic electrode Ag/AgCl interacts selectively with Cl^- ions in the electrolyte and the cationic electrode of a defective $Na_{2-x}Mn_5O_{10}$ nanorod interacts with Na^+ ions selectively. A typical 4-step cycle of this battery is schematically shown in Fig. 37a to show how energy extraction can be accomplished. The electrodes are initially kept in a low NaCl concentration solution (*i.e.,* river water) in their discharged states, the Na^+ and Cl^- ions are gradually removed from the respective electrodes to keep equilibrium between the electrolyte and the respective electrode (Step 1, charging). By exchanging the electrolyte to seawater (a high concentration solution) (Step 2), Na^+ and Cl^- ions are gradually electrosorbed into the respective electrodes (Step 3). Finally, NaCl concentration of seawater decreases to a low level (similar to that of the river wa-

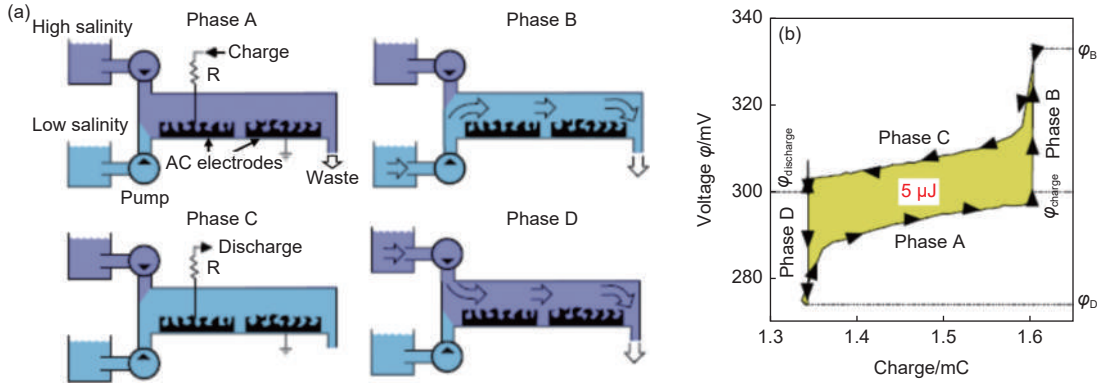

Fig. 36 Cycle for extracting energy from salinity difference: (a) scheme of the four phases of the cycle and (b) the potential *vs.* charge relation during cycling. An extracted energy in this case is 5 μJ. Reprinted with permission from Ref. [75]. Copyright (2009) by Elsevier

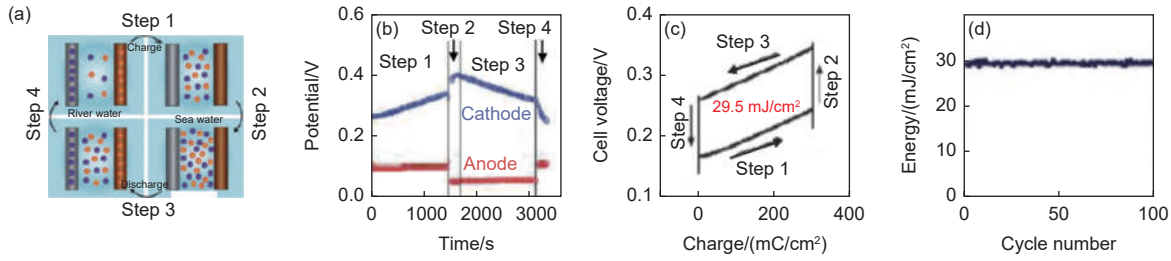

Fig. 37 A "mixing entropy battery" using NaCl water with different concentrations (river water and seawater): (a) schematic illustration of the working principle of the battery, (b) change in cell potential in a cycle, (c) change the cell potential with cell charge, the defined area being equal to the extracted energy, and (d) cycle stability for energy extraction. Reprinted with permission from Ref. [76]. Copyright (2011) by Elsevier

ter), *i.e.*, going back to the beginning. The changes in the cell potential at each step are shown in Fig. 37b. Since the open circuit potential for the cell increases with the concentration of NaCl, the cell potential increases with time due to the NaCl concentration increase by transfering ions from the electrodes to the electrolyte to keep an equilibrium between the electrolyte and the respective electrodes (Step 1). By exchanging the electrolyte to the sea water (Step 2), the cell potential increases slightly, but it decreases due to the reversed transfer of ions from the electrolyte to the respective electrodes (Step 3, discharging) to keep an equilibrium between the electrolyte and the electrodes. By rewriting Fig. 37b and c as the relation between the cell potential and charge, the extracted energy is calculated to be about 29 mJ/cm^2 per cycle. The extraction of energy from the NaCl concentration difference could be stably achieved up to 100 cycles (Fig. 37d). The cell composed from a couple of AgCl and $Li_{1-x}FePO_4$ with LiCl electrolyte was studied and a higher extracted energy of about 38 mJ/cm^2 was obtained[76]. The same systems called "desalination battery" using NaCl and LiCl electrolytes are reported[77–78]. A system using λ-MnO_2 positive electrode and AgCl negative electrode was proposed for Li recovery[79]. Copper hexacyanoferrate (CuHCF, $C_6Cu_4FeN_6$) was also employed for the electrodes[80–81].

A stack consisting of 8 parallel M-CDI cells of the graphite current collectors (thickness of 250 μm), the commercial AC electrodes (270 μm thick) with CEM and AEM (~160 μm thick) with a polymer spacer (400 μm) was investigated[82]. By alternating the flows of saline and fresh water through the cell allowed automatic electric power-generation owing to water salinity differences.

5 Concluding remarks

A novel concept to evaluate CDI performance was proposed, called the CDI Ragone plot, *i.e.*, a plot of SAR (in the unit of mg/g·min) against SAC (mg/g), as shown in Fig. 38 although it has not been employed often[83]. For the energy storage electrochemical devices (*i.e.*, supercapacitor and batteries) Ragone plot, *i.e.*, the plot of power density (in the unit of W/kg) against energy density (Wh/kg) has been commonly used. This plot can facilitate the optimization of the parameters for CDI processes. From the com-

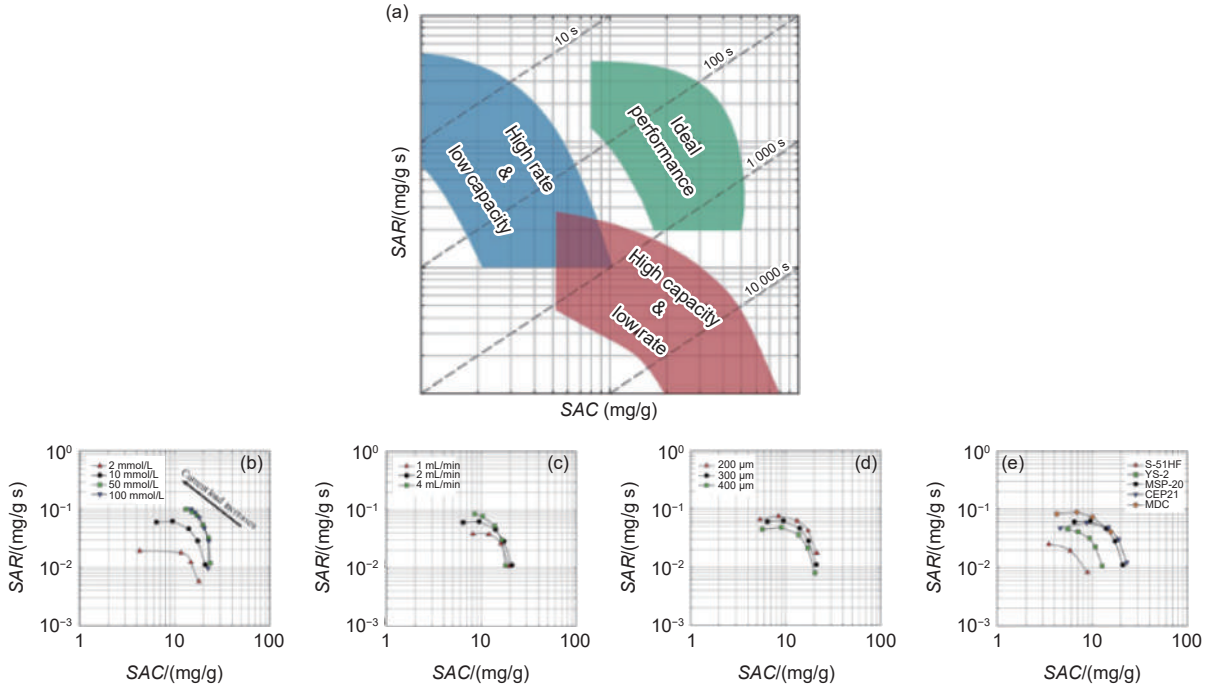

Fig. 38　CDI ragone plots for CDI performance[83]: (a) A conceptual diagram of a CDI Ragone plot. Effect of various parameters on the CDI Ragone plot. Each plot shows the effect of the (b) salt concentration, (c) flow rate, (d) electrode thickness, and (e) type of carbon material

parative study on various parameters using the CDI Ragone plot, such as salt concentration, flow rate, carbon materials and thickness of the electrodes, the optimal conditions can be suggested for the best desalination performance in terms of the SAC and SAR, as shown examples in Fig. 38b-e. In the CDI Ragone plot, an upper, right-side shift is favorable because it indicates a higher SAC and SAR (Fig. 38a).

For practical applications for water desalination, the flowing electrodes (FE)-CDI cell seems to be the most promising, mainly because desalination can perform continuously, although the selection of the cell type depends strongly on the local situations, such as the drinking water scarcity, electric power supply, etc. Particularly the introduction of the short-circuited closed-cycle (SCC) operation mode in FE-cell system, instead of the isolated closed-cycle (ICC) operation (Fig. 28b), makes the operation cost lower. For FE-cell, the determination of the parameters of SAC, SAR and CE is difficult and so difficult to compare the CDI performances with other type cells. In addition, the fundamental and sufficient experimental experiences on the FE cells are not yet accumulated. For the FE cells, following specific parameters for their operation have to be optimized, in addition to the parameters applied commonly on other types of CDI cells, such as the flowing conditions of the brackish solution, the concentrations of salts and flowing rate, applied voltage between the electrodes.

(1) Carbon materials for the flowing electrodes, including their pore structure and particle size. Regrettably only a limited number of carbon materials had been studied for FE cells, such as the commercially available activated carbons, carbon blacks and so on, although there are so many kinds of carbon materials with different particle sizes and morphologies.

(2) Flowing electrolyte solution suspended flowing carbon electrode, what solvent, concentration of electrode carbon, flowing rate, etc.

Since these parameters are strongly related with each other, certain number of experimental points are demanded. The discussion on the bases of Ragone plots for each of these parameters (Fig. 38) may lead to sufficient determination of the most optimal operation conditions of FE cells.

References

[1] Gao M, Zhu L, Peh C K, et al. Solar absorber material and system designs for photothermal water vaporization towards clean water and energy production[J]. Energy & Environmental Science, 2019, 12(3): 841-864.

[2] Huang Z H, Yang Z, Kang F, et al. Carbon electrodes for capacitive deionization[J]. Journal of Materials Chemistry A, 2017, 5(2): 470-496.

[3] Zhang C, He D, Ma J, et al. Faradaic reactions in capacitive deionization (CDI)-problems and possibilities: A review[J]. Water Research, 2018, 128: 314-330.

[4] Tang W, Liang J, He D, et al. Various cell architectures of capacitive deionization: Recent advances and future trends[J]. Water Research, 2019, 150: 225-251.

[5] Anis S F, Hashaikeh R, Hilal N. Functional materials in desalination: A review[J]. Desalination, 2019, 468: 114077.

[6] Kim N, Lee J, Kim S, et al. Short review of multichannel membrane capacitive deionization: principle, current status, and future prospect[J]. Applied Sciences, 2020, 10(2): 683.

[7] Vafakhah S, Beiramzadeh Z, Saeedikhani M, et al. A review on free-standing electrodes for energy-effective desalination: Recent advances and perspectives in capacitive deionization[J]. Desalination, 2020, 493: 114662.

[8] Xing W, Liang J, Tang W, et al. Versatile applications of capacitive deionization (CDI)-based technologies[J]. Desalination, 2020, 482: 114390.

[9] Oladunni J, Zain J H, Hai A, et al. A comprehensive review on recently developed carbon based nanocomposites for capacitive deionization: From theory to practice[J]. Separation and Purification Technology, 2018, 207: 291-320.

[10] Nakayama Y, Imamura E, Noda S. Capacitive deionization characteristics of compressed granular activated carbon[J]. Separation and Purification Technology, 2021, 277: 119454.

[11] Qiang H, Shi M, Wang F, et al. Green synthesis of high N-doped hierarchical porous carbon nanogranules with ultra-high specific surface area and porosity for capacitive deionization[J]. Separation and Purification Technology, 2023, 308: 122918.

[12] Liu M, Xu M, Xue Y, et al. efficient capacitive deionization using natural basswood-derived, freestanding, hierarchically porous carbon electrodes[J]. ACS Applied Materials & Interfaces, 2018, 10(37): 31260-31270.

[13] Zheng S M, Yuan Z H, Dionysiou D D, et al. Silkworm cocoon waste-derived nitrogen-doped hierarchical porous carbon as robust electrode materials for efficient capacitive desalination[J]. Chemical Engineering Journal, 2023, 458: 141471.

[14] Zhao C, Wang Q, Chang S, et al. Efficient transport system of cultivated mushroom mycelium enables its derived carbon with high performance electrochemical desalination capability[J].

Carbon, 2022, 196: 699-707.

[15] Stephanie H, Mlsna T E, Wipf D O. Functionalized biochar electrodes for asymmetrical capacitive deionization[J]. Desalination, 2021, 516: 115240.

[16] Song X, Fang D, Huo S, et al. 3D-ordered honeycomb-like nitrogen-doped micro –mesoporous carbon for brackish water desalination using capacitive deionization[J]. Environmental Science: Nano, 2021, 8(8): 2191-2203.

[17] Guo J, Xu X, Hill J P, et al. Graphene–carbon 2D heterostructures with hierarchically-porous P, N-doped layered architecture for capacitive deionization[J]. Chemical Science, 2021, 12(30): 10334-10340.

[18] Halabaso E R, Salvacion J W L, Kuncoro E P, et al. Highly efficient capacitive deionization of brackish water with manganese vanadate nanorod decorated reduced graphene oxide electrode[J]. Environmental Science:Nano, 2021, 8(10): 2844-2854.

[19] Song X, Fang D, Huo S, et al. Exceptional capacitive deionization desalination performance of hollow bowl-like carbon derived from MOFs in brackish water[J]. Separation and Purification Technology, 2021, 278: 119550.

[20] Kyaw H H, Myint M T Z, Al-Harthi S, et al. Electric field enhanced in situ silica nanoparticles grafted activated carbon cloth electrodes for capacitive deionization[J]. Separation and Purification Technology, 2022, 281: 119888.

[21] Zong M, Huo S, Liu Y, et al. Hydrangea-like nitrogen-doped porous carbons derived from NH_2-MIL-53(Al) for high-performance capacitive deionization[J]. Separation and Purification Technology, 2021, 256: 117818.

[22] Hu B, Shang X, Nie P, et al. Lithium ion sieve modified three-dimensional graphene electrode for selective extraction of lithium by capacitive deionization[J]. Journal of Colloid and Interface Science, 2022, 612: 392-400.

[23] Bai Y, Huang Z H, Yu X L, et al. Graphene oxide-embedded porous carbon nanofiber webs by electrospinning for capacitive deionization[J]. Colloids and Surfaces A:Physicochemical and Engineering Aspects, 2014, 444: 153-158.

[24] Wang G, Dong Q, Wu T, et al. Ultrasound-assisted preparation of electrospun carbon fiber/graphene electrodes for capacitive deionization: Importance and unique role of electrical conductivity[J]. Carbon, 2016, 103: 311-317.

[25] Liu Y, Du X, Wang Z, et al. Layered double hydroxide coated electrospun carbon nanofibers as the chloride capturing electrode for ultrafast electrochemical deionization[J]. Journal of Colloid and Interface Science, 2022, 609: 289-296.

[26] Chen C, Men L, Liu A, et al. Enhanced electrochemical and capacitive deionization performances of single-layer graphene oxide/nitrogen-doped porous carbon/activated carbon fiber composite electrodes[J]. Journal of Environmental Chemical Engineering, 2022, 10(6): 108696.

[27] Nie P, Wang S, Shang X, et al. Self-supporting porous carbon nanofibers with opposite surface charges for high-performance inverted capacitive deionization[J]. Desalination, 2021, 520: 115340.

[28] Hameed R M A, Zouli N, Abutaleb A, et al. Improving water desalination performance of electrospun carbon nanofibers by supporting with binary metallic carbide nanoparticles[J]. Ceramics International, 2022, 48(4): 4741-4753.

[29] Wang P, Ma W, Xue S, et al. N-doped carbon nanosheets assembled microspheres for more effective capacitive deionization[J]. Separation and Purification Technology, 2021, 276: 119336.

[30] Gong X, Luo W, Guo N, et al. Carbon nanofiber@ZIF-8 derived carbon nanosheet composites with a core–shell structure boosting capacitive deionization performance[J]. Journal of Materials Chemistry A, 2021, 9(34): 18604-18613.

[31] Talebi M, Ahadian M M, Shahrokhian S. Binder-free 3D graphene nanostructures on Ni foam substrate for application in capacitive deionization[J]. Diamond and Related Materials, 2021, 120: 108612.

[32] Zhang G, Li W, Chen Z, et al. Freestanding N-doped graphene membrane electrode with interconnected porous architecture for efficient capacitive deionization[J]. Carbon, 2022, 187: 86-96.

[33] Zhang H, Wang C, Zhang W, et al. Nitrogen, phosphorus co-doped eave-like hierarchical porous carbon for efficient capacitive deionization[J]. Journal of Materials Chemistry A, 2021, 9(21): 12807-12817.

[34] Lee J H, Bae W S, Choi J H. Electrode reactions and adsorption/desorption performance related to the applied potential in a capacitive deionization process[J]. Desalination, 2010, 258(1): 159-163.

[35] Choi J-H. Determination of the electrode potential causing Faradaic reactions in membrane capacitive deionization[J]. Desalination, 2014, 347: 224-229.

[36] Bouhadana Y, Avraham E, Noked M, et al. Capacitive deionization of NaCl solutions at non-steady-state conditions: Inversion functionality of the carbon electrodes[J]. The Journal of Physical Chemistry C, 2011, 115(33): 16567-16573.

[37] Cohen I, Avraham E, Bouhadana Y, et al. Long term stability of capacitive de-ionization processes for water desalination: The challenge of positive electrodes corrosion[J]. Electrochimica Acta, 2013, 106: 91-100.

[38] He D, Wong C E, Tang W, et al. Faradaic reactions in water desalination by batch-mode capacitive deionization[J]. Environmental Science & Technology Letters, 2016, 3(5): 222-226.

[39] Taha M M, Anwar S E, Ramadan M, et al. Controlled fabrication of mesoporous electrodes with unprecedented stability for water capacitive deionization under harsh conditions in large size cells[J]. Desalination, 2021, 511: 115099.

[40] Adorna J, Borines M, Dang V D, et al. Coconut shell derived activated biochar –manganese dioxide nanocomposites for high performance capacitive deionization[J]. Desalination, 2020, 492: 114602.

[41] Wang H, Edaño L, Valentino L, et al. Capacitive deionization using

carbon derived from an array of zeolitic-imidazolate frameworks[J]. Nano Energy, 2020, 77: 105304.

[42] Tang W, He D, Zhang C, et al. Comparison of Faradaic reactions in capacitive deionization (CDI) and membrane capacitive deionization (MCDI) water treatment processes[J]. Water Research, 2017, 120: 229-237.

[43] Juchen P T, Barcelos K M, Oliveira K S G C, et al. Using crude residual glycerol as precursor of sustainable activated carbon electrodes for capacitive deionization desalination[J]. Chemical Engineering Journal, 2022, 429: 132209.

[44] Son J W, Choi J H. Suppression of electrode reactions and enhancement of the desalination performance of capacitive deionization using a composite carbon electrode coated with an ion-exchange polymer[J]. Separation and Purification Technology, 2021, 278: 119503.

[45] Li H, Zou L. Ion-exchange membrane capacitive deionization: A new strategy for brackish water desalination[J]. Desalination, 2011, 275(1): 62-66.

[46] Biesheuvel P M, van der Wal A. Membrane capacitive deionization[J]. Journal of Membrane Science, 2010, 346(2): 256-262.

[47] Lee J B, Park K K, Eum H M, et al. Desalination of a thermal power plant wastewater by membrane capacitive deionization[J]. Desalination, 2006, 196(1): 125-134.

[48] Porada S, Sales B B, Hamelers H V M, et al. Water desalination with wires[J]. The Journal of Physical Chemistry Letters, 2012, 3(12): 1613-1618.

[49] Suss M E, Baumann T F, Bourcier W L, et al. Capacitive desalination with flow-through electrodes[J]. Energy & Environmental Science, 2012, 5(11): 9511-9519.

[50] Baumann T F, Worsley M A, Han T Y J, et al. High surface area carbon aerogel monoliths with hierarchical porosity[J]. Journal of Non-Crystalline Solids, 2008, 354(29): 3513-3515.

[51] Wang G, Qian B, Wang Y, et al. Electrospun porous hierarchical carbon nanofibers with tailored structures for supercapacitors and capacitive deionization[J]. New Journal of Chemistry, 2016, 40(4): 3786-3792.

[52] Remillard E M, Shocron A N, Rahill J, et al. A direct comparison of flow-by and flow-through capacitive deionization[J]. Desalination, 2018, 444: 169-177.

[53] Zhang C, He D, Ma J, et al. Comparison of faradaic reactions in flow-through and flow-by capacitive deionization (CDI) systems[J]. Electrochimica Acta, 2019, 299: 727-735.

[54] Zhang X, Dutta J. X-Fe (X = Mn, Co, Cu) Prussian blue analogue-modified carbon cloth electrodes for capacitive deionization[J]. ACS Applied Energy Materials, 2021, 4(8): 8275-8284.

[55] Reale E R, Regenwetter L, Agrawal A, et al. Low porosity, high areal-capacity prussian blue analogue electrodes enhance salt removal and thermodynamic efficiency in symmetric Faradaic deionization with automated fluid control[J]. Water Research X, 2021, 13: 100116.

[56] Shi M, Qiang H, Chen C, et al. Construction and evaluation of a novel three-electrode capacitive deionization system with high desalination performance[J]. Separation and Purification Technology, 2021, 273: 118976.

[57] Laxman K, Myint M T Z, Al Abri M, et al. Desalination and disinfection of inland brackish ground water in a capacitive deionization cell using nanoporous activated carbon cloth electrodes[J]. Desalination, 2015, 362: 126-132.

[58] Jeon S I, Park H R, Yeo J G, et al. Desalination via a new membrane capacitive deionization process utilizing flow-electrodes[J]. Energy & Environmental Science, 2013, 6(5): 1471-1475.

[59] Jeon S i, Yeo J g, Yang S, et al. Ion storage and energy recovery of a flow-electrode capacitive deionization process[J]. Journal of Materials Chemistry A, 2014, 2(18): 6378-6383.

[60] He C, Ma J, Zhang C, et al. Short-circuited closed-cycle operation of flow-electrode CDI for brackish water softening[J]. Environmental Science & Technology, 2018, 52(16): 9350-9360.

[61] Ma J, Ma J, Zhang C, et al. Water recovery rate in short-circuited closed-cycle operation of flow-electrode capacitive deionization (FCDI)[J]. Environmental Science & Technology, 2019, 53(23): 13859-13867.

[62] Yang S, Choi J, Yeo J G, et al. Flow-electrode capacitive deionization using an aqueous electrolyte with a high salt concentration[J]. Environmental Science & Technology, 2016, 50(11): 5892-5899.

[63] Yang S, Kim H, Jeon S I, et al. Analysis of the desalting performance of flow-electrode capacitive deionization under short-circuited closed cycle operation[J]. Desalination, 2017, 424: 110-121.

[64] Ma J, Liang P, Sun X, et al. Energy recovery from the flow-electrode capacitive deionization[J]. Journal of Power Sources, 2019, 421: 50-55.

[65] Doornbusch G J, Dykstra J E, Biesheuvel P M, et al. Fluidized bed electrodes with high carbon loading for water desalination by capacitive deionization[J]. Journal of Materials Chemistry A, 2016, 4(10): 3642-3647.

[66] Xu L, Mao Y, Zong Y, et al. Membrane-current collector-based flow-electrode capacitive deionization system: A novel stack configuration for scale-up desalination[J]. Environmental Science & Technology, 2021, 55(19): 13286-13296.

[67] Xu L, Ding R, Mao Y, et al. Selective recovery of phosphorus and urea from fresh human urine using a liquid membrane chamber integrated flow-electrode electrochemical system[J]. Water Research, 2021, 202: 117423.

[68] Gao X, Omosebi A, Landon J, et al. Surface charge enhanced carbon electrodes for stable and efficient capacitive deionization using inverted adsorption –desorption behavior[J]. Energy & Environmental Science, 2015, 8(3): 897-909.

[69] Lee J Y, Seo S J, Yun S H, et al. Preparation of ion exchanger layered electrodes for advanced membrane capacitive deionization (MCDI)[J]. Water Research, 2011, 45(17): 5375-5380.

[70] Lee J, Jo K, Lee J, et al. Rocking-chair capacitive deionization for

continuous brackish water desalination[J]. ACS Sustainable Chemistry & Engineering, 2018, 6(8): 10815-10822.

[71] Lee J, Kim S, Kim C, et al. Hybrid capacitive deionization to enhance the desalination performance of capacitive techniques[J]. Energy & Environmental Science, 2014, 7(11): 3683-3689.

[72] Smith K C, Dmello R. Na-ion desalination (NID) enabled by Na-blocking membranes and symmetric na-intercalation: Porous-electrode modeling[J]. Journal of the Electrochemical Society, 2016, 163(3): A530.

[73] Kim N, Jeon J, Elbert J, et al. Redox-mediated electrochemical desalination for waste valorization in dairy production[J]. Chemical Engineering Journal, 2022, 428: 131082.

[74] Ahn D, Kim D, Park J H, et al. Enhanced desalination performance of nitrogen-doped porous carbon electrode in redox-mediated deionization[J]. Desalination, 2021, 520: 115333.

[75] Brogioli D. Extracting renewable energy from a salinity difference using a capacitor[J]. Physical Review Letters, 2009, 103(5): 058501.

[76] La Mantia F, Pasta M, Deshazer H D, et al. Batteries for efficient energy extraction from a water salinity difference[J]. Nano Letters, 2011, 11(4): 1810-1813.

[77] Pasta M, Wessells C D, Cui Y, et al. A desalination battery[J]. Nano Letters, 2012, 12(2): 839-843.

[78] Pasta M, Battistel A, La Mantia F. Batteries for lithium recovery from brines[J]. Energy & Environmental Science, 2012, 5(11): 9487-9491.

[79] Lee J, Yu S-H, Kim C, et al. Highly selective lithium recovery from brine using a λ-MnO_2–Ag battery[J]. Physical Chemistry Chemical Physics, 2013, 15(20): 7690-7695.

[80] Kim T, Rahimi M, Logan B E, et al. Harvesting energy from salinity differences using battery electrodes in a concentration flow cell[J]. Environmental Science & Technology, 2016, 50(17): 9791-9797.

[81] Kim T, Gorski C A, Logan B E. Low energy desalination using battery electrode deionization[J]. Environmental Science & Technology Letters, 2017, 4(10): 444-449.

[82] Sales B B, Saakes M, Post J W, et al. Direct power production from a water salinity difference in a membrane-modified supercapacitor flow cell[J]. Environmental Science & Technology, 2010, 44(14): 5661-5665.

[83] Kim T, Yoon J. CDI ragone plot as a functional tool to evaluate desalination performance in capacitive deionization[J]. RSC Advances, 2015, 5(2): 1456-1461.